Front. Optoelectron. 2018, 11(1): 2–22
https://doi.org/10.1007/s12200-017-0753-1

REVIEW ARTICLE

Two-dimensional material functional devices enabled by direct laser fabrication

Tieshan YANG, Han LIN, Baohua JIA (✉)

Centre for Micro-Photonics, Faculty of Science, Engineering and Technology, Swinburne University of Technology, Hawthorn, Victoria 3122, Australia

Abstract During the past decades, atomically thin, two-dimensional (2D) layered materials have attracted tremendous research interest on both fundamental properties and practical applications because of their extraordinary mechanical, thermal, electrical and optical properties, which are distinct from their counterparts in the bulk format. Various fabrication methods, such as soft-lithography, screen-printing, colloidal-templating and chemical/dry etching have been developed to fabricate micro/nanostructures in 2D materials. Direct laser fabrication with the advantages of unique three-dimensional (3D) processing capability, arbitrary-shape designability and high fabrication accuracy up to tens of nanometers, which is far beyond the optical diffraction limit, has been widely studied and applied in the fabrication of various micro/nanostructures of 2D materials for functional devices. This timely review summarizes the laser-matter interaction on 2D materials and the significant advances on laser-assisted 2D materials fabrication toward diverse functional photonics, optoelectronics, and electrochemical energy storage devices. The perspectives and challenges in designing and improving laser fabricated 2D materials devices are discussed as well.

Keywords two-dimensional (2D) materials, direct laser fabrication, laser thinning, laser doping, photonics and optoelectronics devices, electrochemical energy storage

1 Introduction

Two-dimensional (2D) materials usually refer to crystalline materials consisting of mono or a few layers of atoms, with thicknesses varying from one atomic layer to more than ten nanometers [1–7]. So far, a variety of 2D materials have been successfully isolated, including graphene, hexagonal boron nitride (hBN), transition metal dichalcogenides (TMDCs), including MX_2 (M = Mo, W; X = S, Se, Te), black phosphorus (BP) and perovskite ($MAPbX_3$, MA = CH_3NH_3, X = I, Br) [2,8–15]. Consisting of only one or a few atomic layers, 2D materials exhibit exotic physical and chemical properties, such as atomic thickness, 2D laminar structure and relatively large surface area, which are distinctively different from their bulk counterparts, opening new opportunities for nanoscale devices, especially electronic and photonics applications.

Functional micro/nanoscale devices based on 2D materials have been explored using various fabrication techniques, including soft-lithography [16], screen-printing [17], colloidal-templating [18] and chemical/dry etching [19] in order to utilize the intriguing properties of the 2D materials. Direct laser fabrication has been established as a nanometer patterning enabler for challenges that are otherwise not possible to overcome in diversified fundamental and application settings, because of its unique 3D processing capability, flexible patterning designability and high fabrication accuracy (tens of nanometers), far beyond the optical diffraction limit [20–22]. Recently, this flexible fabrication tool has been widely used in 2D materials patterning, modification, doping and functionalization, demonstrating versatile property. So far, several review papers have provided timely updates on 2D material development and some conceptual device designs [23–29]. As an emerging tool for effective fabrication of 2D material-based functional devices, direct laser processing is getting significant attention due to its enormous flexibility and accuracy. This timely review provides an in-depth summary and understanding on direct laser fabricated 2D material functional devices, which has not been available before.

In this paper, we review the state-of-the-art 2D material-based functional devices using the direct laser fabrication

Received August 7, 2017; accepted September 29, 2017

E-mail: bjia@swin.edu.au

technique. We first provide a brief overview on the physical property changes of 2D materials upon laser exposure. Then, we analyze in detail the advantages and limitations of 2D materials functional devices fabricated by direct laser processing for practical applications, based on the benchmark theoretical and experimental results in this field. Finally, we discuss the remaining challenges and future opportunities in this field.

2 Laser and 2D materials interactions

Depending on laser conditions, laser-matter interactions may involve several concurrent processes: single photon absorption, material ablation, melting and agglomeration of nanostructures and chemical/physical modifications [29,30]. These processes lead to different material property changes, which are the fundamental basis for various device designs.

2.1 Direct laser writing of graphene patterns

Nanofabrication of graphene patterns with high quality on desired substrates remains as the main challenge for future graphene applications and has recently become a focus. The direct laser writing (DLW) technique has been proposed and appears to be a promising approach. Compared with the conventional "synthesis + patterning" approaches, which require multiple processing steps, time-consuming and lack of economic viability, the DLW method provides high flexibility for arbitrary graphene patterning via a non-contact and mask free fabrication process which reduces the fabrication cost. More importantly, DLW can achieve a single-step fabrication of graphene patterns by combining graphene growth and patterning steps, resulting in a significantly enhanced efficiency. In this regard, Xiong et al. reported that bilayer graphene can be synthesized through rapid heating of co-sputtered Ni/C thin films on various insulating substrates, as shown in Fig. 1(a) [31,32]. By applying a femtosecond laser (780 nm, 120 fs, 100 MHz) direct writing technique, open-air and room-temperature nanofabrication of arbitrary graphene patterns on insulating substrates (e.g., glasses and SiO_2/Si) has been established. The method enables the cost-effective fabrication of graphene patterns directly on insulating substrates without a subsequent graphene transfer process. Figure 1(b) shows the graphene pattern of a "G" character under an optical microscope. By simply using a computer program, arbitrary 2D graphene patterns can be designed and fabricated using the DLW system. Figure 1(c) presents the 2D band Raman mapping image of the corresponding graphene pattern, which clearly shows the deposition of graphene patterns on the glass substrate. The uniform color contrast of the Raman image indicates the uniform growth of graphene ribbon by the DLW process.

Another example using DLW method for the fabrication of graphene patterns is the laser-induced localized thermal reduction of graphene oxide (GO) films [20,21,33]. To achieve controllable reduction of GO, photo-induced deoxygenation methods (e.g., photo-thermal reduction [34,35] and photochemical reduction [36–38]) have been developed to realize controlled properties of reduced GO (RGO) in the past few years. Compared with conventional thermal and chemical methods, photo-reduction of GO shows the advantages of tunable reduction degree, flexible patterning, high efficiency and low cost. More importantly, it has the flexibility of direct fabrication and integration with various devices. Laser heating caused by irradiation triggers local chemical/physical reactions in GO, such as the breaking of the oxygen-containing bonds and the formation of new chemical bonds with the molecules/

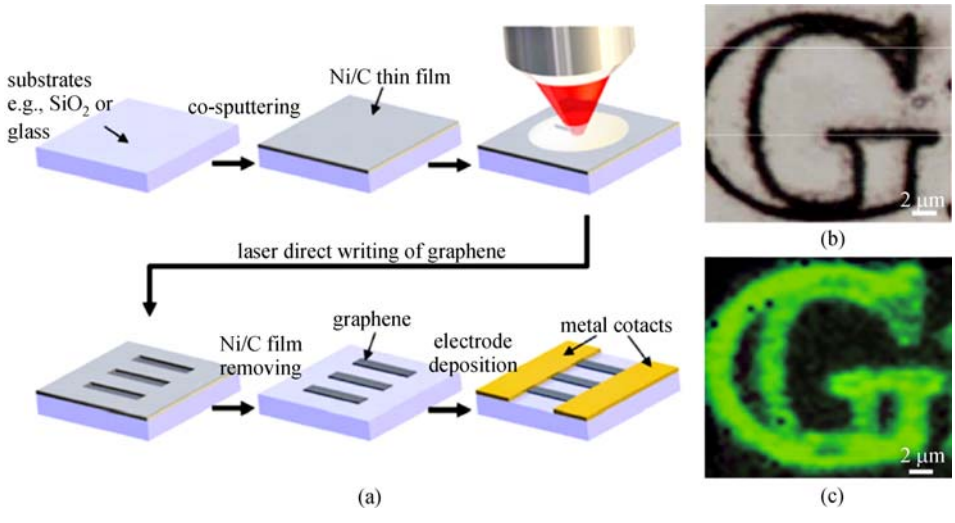

Fig. 1 (a) Experimental schematic of the fabrication process via direct laser writing of graphene patterns in ambient environment; (b) optical and (c) Raman images of the as-fabricated graphene patterns deposited on glass substrates [32]

compounds around the local ambient environment. The transformation from GO to RGO via laser irradiation usually follows two basic processes: 1) photochemical removal of oxygen from the GO surface, which is accompanied by laser ablation; 2) structural reorganization of the newly formed, reduced carbon lattice into the planar, hexagonal, sp^2-conjugated graphene structure [33].

The complex patterns of any arbitrary shapes with a high feature resolution and a small pattern size on integrated graphene materials can be achieved easily by the DLW method. Zhang et al. successfully achieved controllable reduction and patterning of GO films to fabricate graphene microcircuits by using a femtosecond laser (790 nm, 120 fs, 80 MHz), as shown in Fig. 2(a), which is the schematic of the femtosecond DLW reduction and the as-created micropatterns observed by an optical microscope (Fig. 2 (b)) and an atomic force microscope (Fig. 2(c)). Micropatterns with a resolution of 500 nm could be achieved. The mechanism of this femtosecond DLW-induced deoxygenation could be mainly attributed to electronic excitation effect and the electron-hole (*e-h*) recombination-induced thermal effect. During the femtosecond DLW process, the electronic excitation effect is significant in the first several picoseconds, which largely weakens C-O electronic bonding near the top of the valence band, leading to an immediate deoxygenation of GO. After sufficient *e-h* recombination, normal heat reduction becomes dominant [33].

2.2 Laser thinning of 2D materials

TMDCs are intriguing 2D materials that have extraordinary mechanical, electrical and optical properties. For instance, monolayer MoS_2 has a large direct bandgap of ~1.8 eV, while the bulk MoS_2 has an indirect bandgap of 1.2 eV. Therefore, deterministic preparation of a monolayer of MoS_2 is crucial toward exploiting monolayer devices. Although mechanical and chemical exfoliation methods can be used to obtain high quality MoS_2 monolayers, the lack of control in the thickness, shape, size and position of the flakes limits their applications. Castellanos-Gomez et al. used a tightly focused continuous wave (CW) 514 nm laser to thin MoS_2 down to a monolayer, as shown in Fig. 3 [39]. A similar way was also used to process multilayered graphene to obtain a monolayer of graphene [40]. After scanning the focused laser beam on the multilayered sample with an optimized power density and scanning speed, a uniform monolayer region was created. By extending this to large area MoS_2 films grown by the chemical vapor deposition (CVD) method, direct thinning and micro-patterning could be achieved simultaneously. As shown in Fig. 3(a), the sample absorbs the photons and converts the energy into thermal energy. The generated heat facilitates the sublimation of the upper layers to realize the direct thinning and a monolayer domain surrounded by a multilayer region can be fabricated (Fig. 3(c)). The MoS_2 thinning process can be

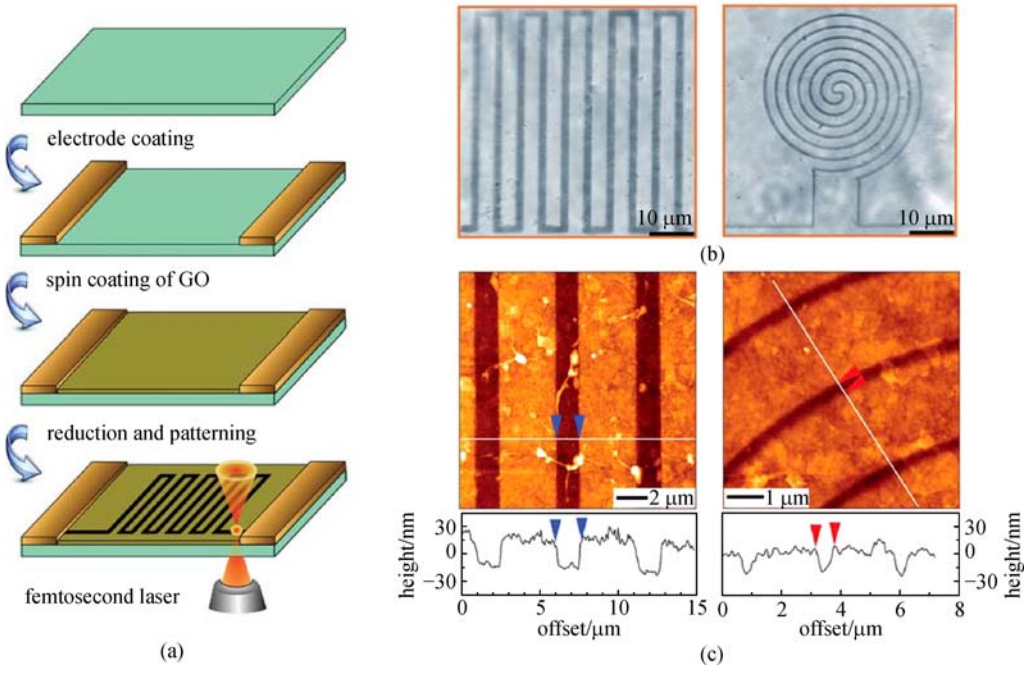

Fig. 2 (a) Schematic illustration of the femtosecond direct laser writing reduction and patterning of GO; (b) optical microscopic images of different micropatterns; (c) atomic force microscopy image of the details of micropatterns, the bottom two images show the profile of the micropatterns [33]

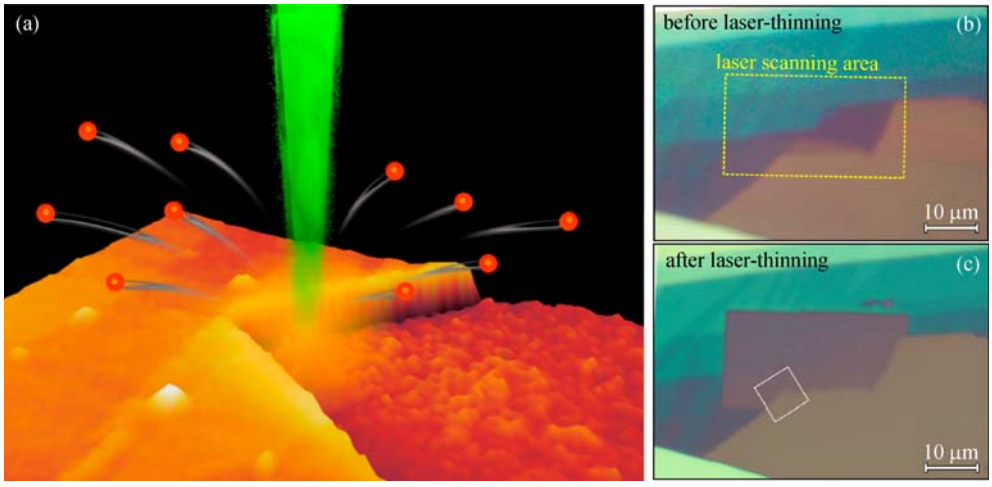

Fig. 3 (a) Schematic of laser interacts with MoS_2 flake; (b) optical microscopic image of a multilayered MoS_2 flake deposited onto a 285 nm SiO_2/Si substrate; (c) same as in (b) after scanning a laser in the area marked by a dashed rectangle in (b). The laser thinning parameters were λ = 514 nm, incident power on the sample 10 mW, scan step 400 nm, and exposure time of 0.1 s between steps [39]

further controlled by choosing the appropriate laser wavelength or using an ultrafast laser. In contrast, monolayer MoS_2 is transparent, implying potential for selective-layer processing. This method has also been applied to directly thinning and patterning WSe_2 [41], $MoTe_2$ [42] and even BP [43]. The thinning mechanism is based on the anisotropic thermal conductivity along the horizontal and vertical directions. The spacing between two adjacent layers function as a good thermal insulating layer, preventing the laser energy to be conducted to the adjacent layer, generating selectivity for thinning. Cho et al. proposed and demonstrated laser thinning process to fabricate an ohmic heterophase homojunction between semiconducting hexagonal (2H) and metallic monoclinic (1T') molybdenum ditelluride ($MoTe_2$) that is stable up to 300°C and increases the carrier mobility of the $MoTe_2$ transistor by a factor of about 50, while retaining a high on/off current ratio of 106, which is beneficial for the electronics devices [42]. In addition to the capabilities of thinning and patterning, this method also possesses the capability to modify the material properties, such as bandgap, optical property, electrical conductivity and surface properties of the TMDCs samples, enabling broad optoelectronic applications [30].

2.3 Laser doping of 2D materials

Laser-assisted doping has been reported to be able to modify semiconductor device characteristics in various 2D materials, leading to superior device properties compared with other conventional methods, such as implantation or diffusion. During the reduction of GO under laser irradiation, a controlled dopant precursor gas environment can facilitate the simultaneous doping of the RGO by taking the advantage of defect sites in GO [26,44]. When the doping process is conducted using a nanosecond laser, ultraviolet wavelength is used due to the strong GO absorption band [45]. A similar process using a femtosecond laser in a controlled ammonia environment showed efficient reduction into *n*-doped graphene [44].

TMDCs materials have direct bandgaps ranging from 1.0 to 2.5 eV [3]. Therefore, a visible wavelength laser matching the absorption band of the material is a good choice for materials processing. For nanoscale devices using ultrathin TMDCs layered materials, to minimize random dopant fluctuation and ensure device performance reproducibility, site-specific doping with a precise doping level control is essential. Laser-assisted phosphorus doping in ultrathin (monolayer and bilayer) TMDCs, including *n*-type MoS_2 and *p*-type WSe_2, was recently demonstrated using a continuous wave 532 nm laser. Such a versatile, air-stable, and tunable method was carried out by varying the duration and intensity of a focused laser beam in a phosphine (PH_3) environment to accomplish the site-specific doping, as shown in Fig. 4(a) [46]. The laser serves two important functions: 1) creation of sulfur vacancies in the TMDC materials; 2) simultaneous dissociation of the dopant molecules. The released dopant molecules are then incorporated into the vacancy sites. Different from its function as *n*-type dopant for silicon, PH_3 was introduced as a *p*-type dopant precursor for ultrathin TMDCs where phosphorus occupies sulfur sites. Figure 4(b) shows the optical image of mechanically exfoliated monolayer and five-layer MoS_2 flakes. The monolayer MoS_2 in Fig. 4(c) is identified with a thickness of ~ 0.7 nm. The photoluminescence (PL) mapping in Fig. 4(d) is taken from the laser-irradiated region indicated in Fig. 4(c). Extending the laser-doping method to emerging 2D materials not only allows site-specific selectivity, but also prevents the redistribution of the impurity profile via a pulsed laser with short

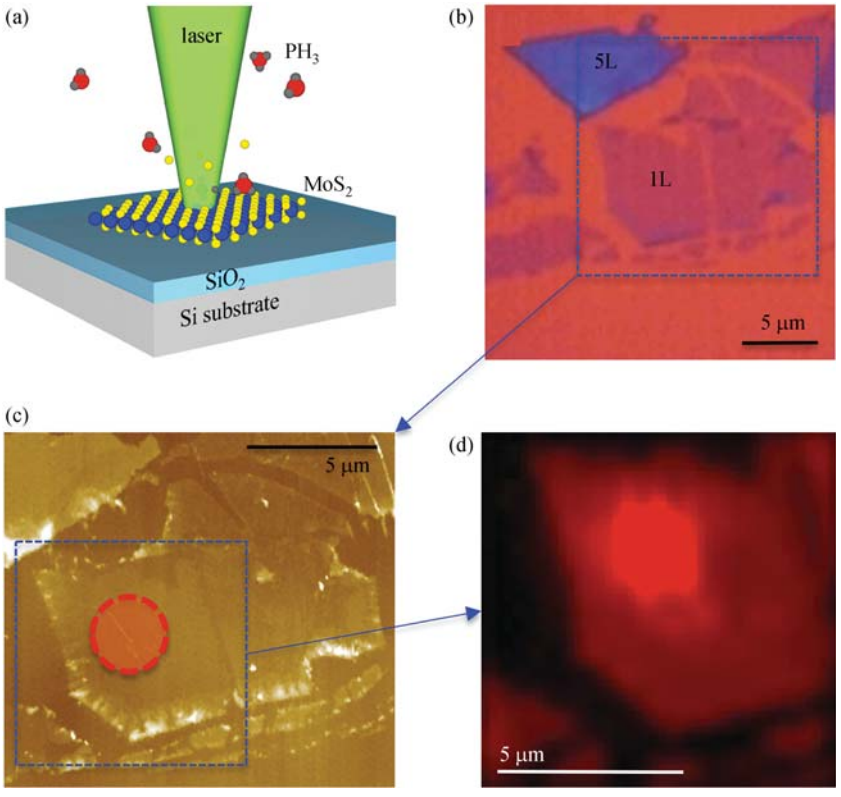

Fig. 4 Laser-assisted doping of MoS_2. (a) Schematic diagram of laser-assisted doping method. Focused laser locally illuminated on the MoS_2 flakes (blue atoms, Mo; yellow atoms, S) located on a SiO_2/Si substrate under diluted phosphine dopant gas environment; (b) optical image of as-prepared monolayer and five-layer MoS_2 on SiO_2/Si substrate (blue color represents MoS_2); (c) AFM image of the zoomed area in (b). Its thickness is ~ 0.7 nm, nm, in a good agreement with the thickness of a monolayer of MoS_2. The circle in (c) is the laser exposed spot area in the laser doping; (d) PL mapping of the zoomed area in (c) that showed the PL intensity enhancement of the laser-assisted doped area [46]

irradiation durations. Moreover, ultrafast laser may provide a novel way for TMDC layer doping through atomic-scale control of vacancy generation and the subsequent refilling with impurity atoms via non-thermal lattice disturbance processes [46].

2.4 Two beam laser interference technique

In addition to DLW, another fabrication method of periodic arrays within the micro- and submicrometer scale is two beam laser interference (TBLI) [33,47,48]. This technique is particularly suitable for periodic pattern fabrication on planar and non-planar surfaces. One obvious advantage of this method is that fairly large areas can be processed within a short period of time. Hence, it offers a route to up-scaled production [49]. By properly selecting the processing parameters, it is suitable to create various surface topographies. Likewise, different effects such as melting, defect and phase formation can be induced. Therefore, electrical, chemical and/or mechanical surface properties can be periodically varied. As shown in Fig. 5, a grating structure with a period of 2 μm was created through the laser ablation and removal of the oxygen-containing functional groups of a GO film [33]. The origin of such a beautiful iridescence could be explained by the light diffraction from the grating. In addition to the 2D grating structure, a nanofolder structure on the edge of the grating patterns was also formed due to the layered arrangement of the GO sheets. These hierarchical structures contribute to a high adhesive superhydrophobic property. Since the periodicity of the grating on the graphene film could be tuned in a certain range by changing the angle between the two laser beams, the optical properties could be manipulated in a controlled manner by changing the laser fabrication parameters [33,47].

3 Broad applications

Laser irradiance introduces local physical and chemical changes of 2D materials, leading to effective property modifications, which provide the basic for many 2D material devices formation with laser processing [29]. For example, the complex refractive index of GO and TMDCs (WS_2) can be changed during the DLW process, which is beneficial for phase modulation in ultrathin 2D materials

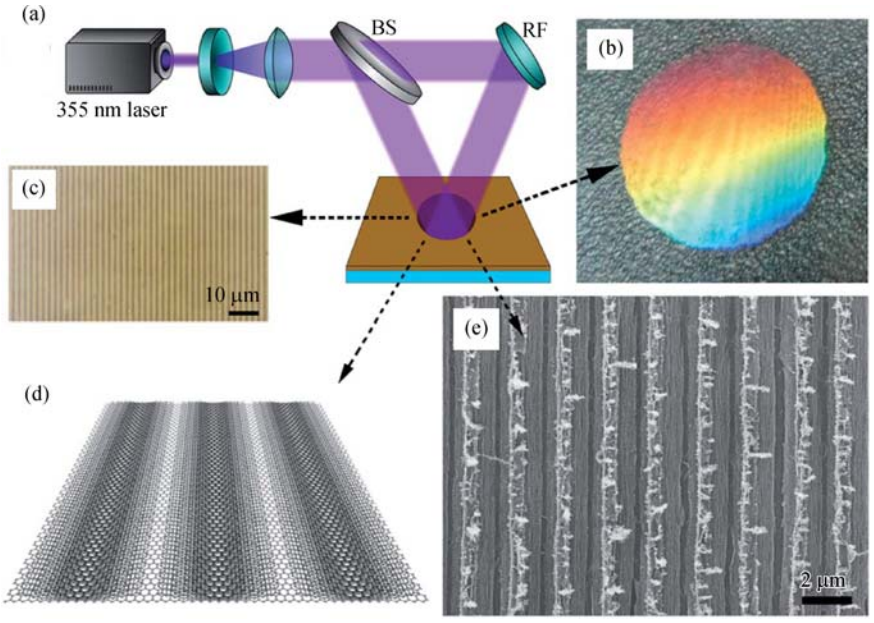

Fig. 5 (a) Schematic illustration of the two-beam laser interference (TBLI) system for the fabrication of superhydrophobic graphene films; (b) photograph of an as-patterned graphene film, the structural color can be observed by the naked eye; (c) optical microscopic image of the graphene pattern; (d) schematic illustration of the graphene surface after the TBLI treatment; (e) scanning electron microscope (SEM) image of the superhydrophobic and iridescent graphene film [33]

lens [22,50,51]. The bandgap and electrical conductivity of 2D materials can be modulated by laser irradiation, which can be used in photonics and optoelectronics devices, like transparent conductive electrode (TCE), light emission diodes (LEDs) and field effect transistors (FETs). Besides, the porosity, surface hydrophilicity or phase can also be changed by laser irradiation, which are suitable for targeted applications, such as electrochemical storage and biocompatible devices. Recently, a number of functional devices have been successfully demonstrated using 2D materials by direct laser processing, indicating its great application potentials.

3.1 Photonics and optoelectronic devices

3.1.1 Ultrathin flat lens

Extensive efforts have been devoted to develop ultrathin flat lens, such as micro Fresnel lenses and conventional micro lenses, plasmonics lenses and metasurface lenses [52]. However, it is still challenging to realize ultrathin optical lenses with subwavelength focusing resolution, high focusing efficiency, broadband wavelength operation, cost-effective manufacturing and flexible integration capability. Zheng et al. designed a novel ultrathin (thickness of ~ 200 nm) flat GO lens based on the manipulation of the phase and amplitude of an incident light beam simultaneously [50,53].

The design of the GO ultrathin flat lens and the corresponding results both in theory and experiment are illustrated in Fig. 6. The GO flat lens with the concentric ring was fabricated by the DLW method to covert the GO to RGO via the photo-reduction process, as illustrated in Fig. 6(a) [50]. The controllable removal of the oxygen-containing functional groups by the laser in the exposed GO film leads to three continuously tunable local physical property variations: the reduction of the film thickness, the increase of the refractive index and the decrease of the transmission. Consequently, the three tunable local property variations provide a flexibility in designing new ultrathin flat lens concept with the capabilities of both amplitude and phase control, and thus make the GO flat lens concept different from the conventional Fresnel lenses and other flat lenses, which mostly rely on either phase or amplitude modulation solely.

When a uniform plane wave impinges on the GO lens, part of the beam is absorbed and refracted by the RGO zones, experiencing substantial amplitude and phase modulations. The other part of the beam propagating through the GO zones only experiences ignorable amplitude modulations (Figs. 6(b) and 6(c)). The subwavelength 3D focusing is a result of the interference of wavelets originated in the lens plane from different zones (Fig. 6(d)), which has been confirmed by its cross-sectional plots in the lateral and axial directions both theoretically and experimentally, as shown in Figs. 6(e)–6(h). To further test its mechanical robustness, a GO thin film with prefabricated lens arrays is integrated on a flexible polydimethylsiloxane (PDMS) substrate. The 4 × 4 GO lens array survives without any compromise of the

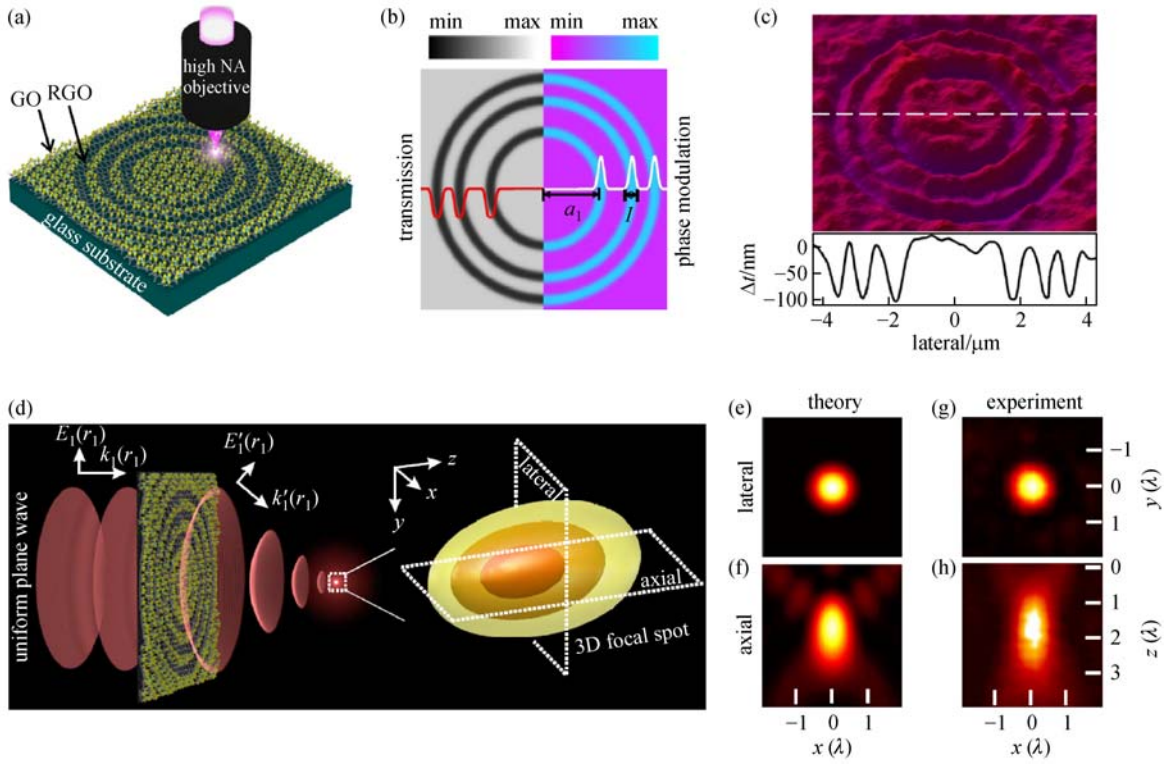

Fig. 6 Design of the GO lens. (a) Conceptual design and laser fabrication of the GO ultrathin lens; (b) amplitude and phase modulations provided by the transmission and refractive index difference, respectively, between the GO and RGO zones; (c) topographic profile of the GO lens measured with an optical profiler; (d) left: schematic of the wavefront manipulation by the GO lens converting the incident plane wave into a spherical wavefront. Right: intensity distributions of the 3D focal spot predicted by the analytical model for a GO lens with three rings and the radius of the most inner rings of 1.8 μm; (e, f) theoretical focal intensity distributions in the lateral and axial directions; (g, h) experimental focal intensity distributions along the lateral and axial directions [50]

morphology or optical performance after the bending test, indicating the prominent mechanical strength and flexibility of the GO films [53].

In summary, Zheng et al. showed an ultrathin GO flat lens with 3D subwavelength focusing that is able to tightly focus broadband light from visible to near infrared (~1500 nm bandwidth) with an absolute focusing efficiency of $>32\%$ over the entire band. These flexible GO lenses are mechanically robust with excellent focusing properties under high stress. The facile and scalable fabrication method enables promising applications for on-chip nanophotonics. The new wavefront shaping concept with laser patterned GO films, provides novel and viable solution for ultra-light-weight, highly efficient, highly integratable and flexible optical systems, opening up new avenues for various multidisciplinary applications including non-invasive 3D biomedical imaging, optical microelectromechanical systems (MEMS) and laboratory-on-chip (LoC) devices [22].

Theoretically, the thickness of a flat lens is limited to a monolayer of 2D materials. However, it is difficult to experimentally achieve such a thickness due to the insufficient phase or amplitude modulation based on the intrinsic refractive index and absorption of the materials when the thickness is reduced to sub-nanometer. Lin et al. demonstrated an ultrathin flat WS_2 lens with a thickness of 7 Å, which was fabricated in a monolayer of WS_2 single crystal via DLW method to selectively ablate the material [51]. Compared with conventional phase modulation principle, they applied the ultra-high refractive index of the material to effectively modulate the amplitude of the incident light to achieve 3D focusing with almost diffraction-limited resolution.

The focusing principle of the monolayer WS_2 lens is schematically illustrated in Fig. 7(a). The collimated incident light experiences strong reflection and low transmission ($<30\%$) at the SiO_2-WS_2 and WS_2-air interface when it impinges the area of WS_2 crystal, due to the high index contrast. Meanwhile, the light goes through the SiO_2-air interface with negligible reflection. Thus, the amplitude of the incident light is effectively modulated by the lens. Figure 7(b) shows the Raman mapping image of the fabricated WS_2 lens. The lens structure composing of four concentric rings fabricated in the triangular shaped monolayer WS_2 crystal can be clearly identified due to the high reflection contrast between the

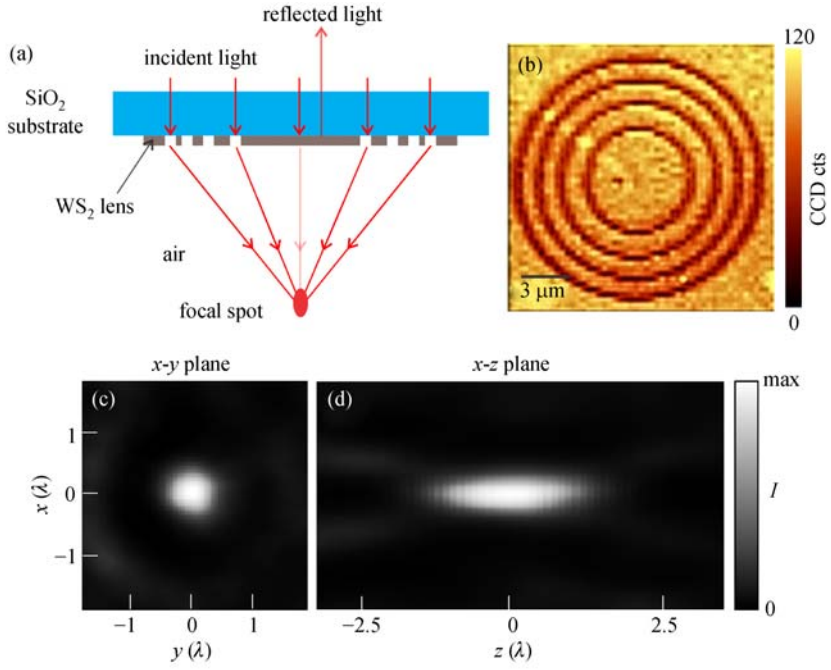

Fig. 7 (a) Schematic demonstration of the focusing principle of the monolayer WS_2 lens; (b) Raman mapping image of a WS2 lens; Cross-sectional intensity distributions of the focal spot in the focal plane (c) and along the axial direction (d) [51]

WS_2 crystal and the SiO_2 substrate. The removal of the WS_2 material in the patterned area is also confirmed. By controlling the position and the line width of the concentric rings, the lens can achieve optimal constructive interference of light at the designed position, which results in a tight focal spot. The cross-sectional images of the focal spot in the *x*-*y* plane and *x*-*z* plane are shown in Figs. 7(c) and 7(d), which present a full width at a half maximum along the *x* and *z*-directions are 0.6λ and 2λ, respectively [51].

3.1.2 Ultrathin GO polarizers

Ultrathin polarizers in the near infrared wavelength range are indispensable elements in integrated optical systems and have been extensively studied using metamaterials, metasurfaces, wire-grid polarizers and guided resonance based polarizers. However, the extinction ratio and the efficiency of the polarizers is largely restricted by the considerable metallic losses, especially in the shorter wavelength for the wire-grid polarizers. The operating wavelengths of the guided resonance-based polarizers are greatly limited to 1550 nm due to the conventional available transparent materials (silicon and indium phosphide) in the infrared range. Moreover, the fabrication and deposition for conventional materials (silicon or metals) are time-consuming. Consequently, it is still challenging to realize ultrathin polarizers from the visible to infrared with a high extinction ratio, high transmission efficiency and flexible capabilities using cost-effective fabrication methods [22,53].

Inspired by the prominent optical properties of GO and laser-induced RGO, Zheng et al. proposed a C-shaped, ultrathin micro-polarizer on a GO film with high a extinction ratio (>3000), which is one order of magnitude larger than the current guided resonance-based polarizer, as shown in Fig. 8 [22]. The periodic C-shaped array on the GO film was designed (Fig. 8(a)), fabricated by DLW method (Fig. 8(b)) [54] and the transmission spectra were calculated for both TM and TE polarizations, respectively (Figs. 8(c) and 8(d)). At the optimized thickness of 100 nm, the GO film can only support the guided resonances at a reasonable linear absorption loss. Notably, the asymmetric Fano resonance can be seen for both polarizations, corresponding to the indirect transmission process where the incident energy excites the guided resonances. Also the direct transmission process has been confirmed by the Febry-Perot oscillation of the background. Moreover, by introducing the C-shaped, asymmetric structure, the spectra is highly sensitive to the incident polarization. For example, a high transmission as large as 0.8 for the TE polarization can be observed at ~ 1.3 μm, whereas almost zero transmission is shown at the same wavelength for the TM polarization due to the strong confinement of the incident light within the C-shaped film (Fig. 8(c)). Consequently, the observed strong polarization sensitivity of the guided resonance on the GO film can potentially serve as an ultrathin planer polarizer [22].

The working wavelength can be tuned over a wide range from the visible (600 nm) to the near infrared (1.6 μm) due to the dispersionless nature of the GO film, largely extending the current working wavelength (1.5 μm) of

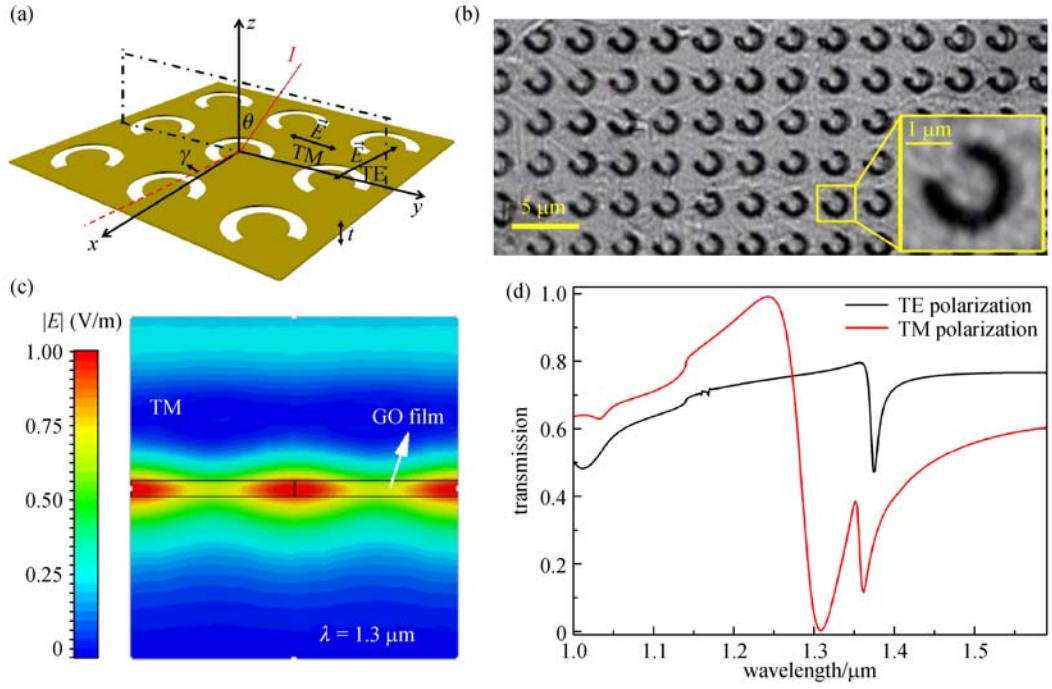

Fig. 8 (a) Schematic design of the proposed GO polarizer with 2D periodic C-shape arrays. The C-shape array is in the *x*-*y* plane and the incident light is in the *y*-*z* plane with the colatitude angle θ; (b) optical microscopic image of fabricated C-shape array. The lattice constant of C-shape array is 3 μm, the line width of each C-shape is 500 nm and the radius of C-shape is 1 μm. Inset: A magnified image of the yellow box; (c) strong confinement of the incident light within the GO polarizer under TM polarization; (d) transmission spectra of the proposed GO polarizer with TE and TM polarized light incidence [22,53]

silicon or indium phosphide materials. Additionally, the incident-angle (θ in Fig. 8(a)) dependence of the micro-polarizer has been studied and high extinction ratio remains for a wide range of θ as large as 30°. Compared to the first graphene fiber polarizer [55], the working principle of the GO polarizer is the guided-mode resonances in a photonic crystal structure. Therefore, the out-of-the-plane incident beam can be polarized by using the GO polarizer, whereas the graphene fiber polarizer is used for the in-plane beam polarization, which means the GO polarizer is useful in free-space optical systems. The GO micro-polarizer may provide various on-chip photonics applications due to its high efficiency, broadband working wavelength range, large extinction ratio and cost-effective fabrication [22,53].

3.1.3 Perfect absorber

Jia et al. demonstrated ultra-broadband transmission light absorber (TLA) of more than 90% at a near infrared wavelength of 1000 nm with a bandwidth of more than 300 nm in ultrathin gratings composed of gradient index graphene-based metamaterials. The 90 nm thick film consisting of alternating GO and dielectric material with 2 nm thickness of each layer is prepared using the layer-by-layer (LBL) self-assembly technique. The gratings structure is fabricated using the flexible femtosecond DLW that simultaneously ablates the film and converts the graphene oxide to graphene via laser photo-reduction. The results are shown in Fig. 9, which open up new avenues for the nanostructured 2D materials photonic device to enable novel optical applications [56].

3.1.4 Creating *p*-*n* junctions in graphene

Owing to the unique physical and chemical properties, graphene shows great potential in various applications, especially in electronics devices, which require precise control of complex patterns of integrated circuits. However, one of the biggest drawbacks of graphene for electronics is its zero band gap. In this regard, construction of *p*-*n* junctions to modulate carrier transmission probability by turning some regions of graphene into *n*-type and others into *p*-type semiconductors is an efficient method to control the current flow. The interfaces between the two regions form *p*-*n* junctions, which are the basic building blocks of semiconductor electronic devices including solar cells, LEDs and FETs [57]. They are considered to be the active sites where the electronic action of the device takes place. This behavior is due to the depletion region of the *p*-*n* junction that enables the flow of electrons in one direction but not the other [29,58].

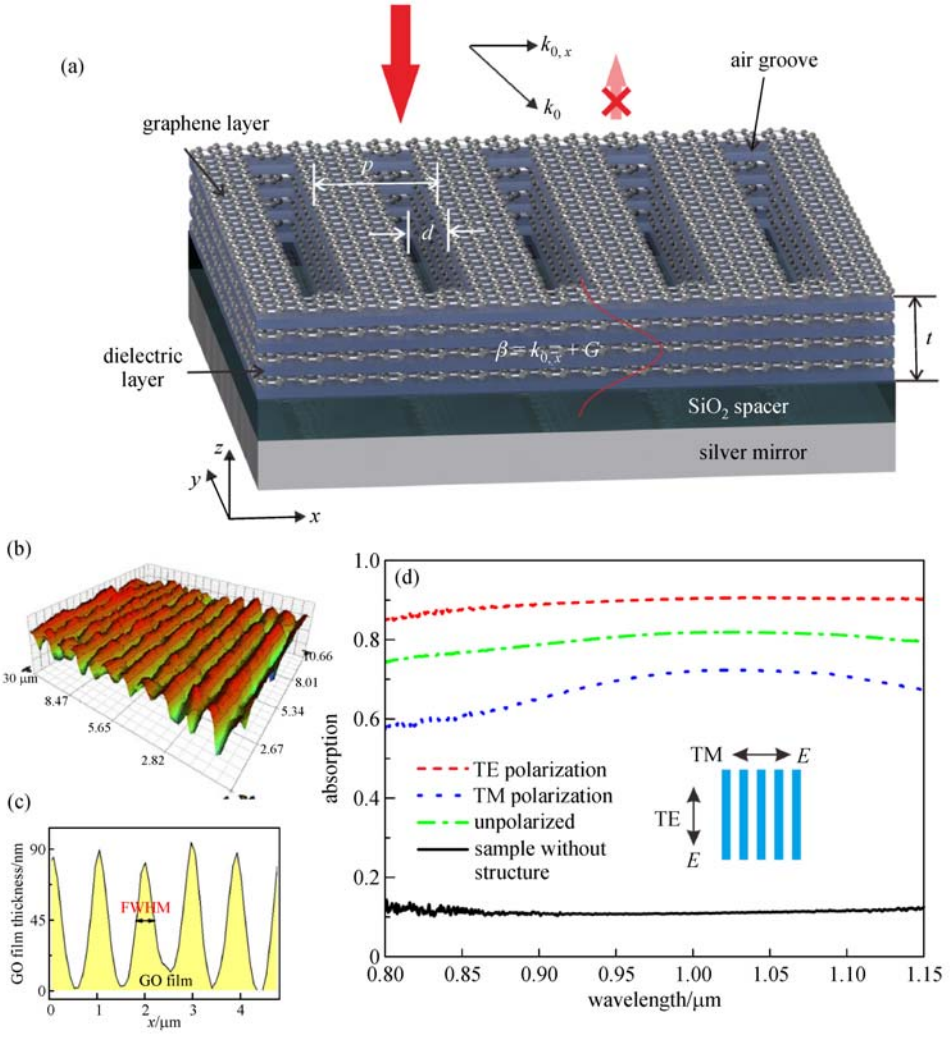

Fig. 9 (a) Schematic representation of a three-layer structure system with the top multilayer graphene-based metamaterial with thickness t patterned as gratings of period p. d is the width of the air groove; (b) optical profiler image of gratings with p = 980 nm and w = 400 nm; (c) cross-sectional plot of the optical profiler image; (d) measured absorption spectra for TE polarization, TM polarization, unpolarized light and sample without grating structure [56]

Seo et al. showed a novel method for doping graphene in air via a simple DLW technique [59]. This method enable the effective control of carrier type and density in graphene, and it can also be used to dope graphene with any arbitrary patterns. When the laser is irradiated to the 6, 13-bis (triisopropylsilylethynyl) pentacene (TIPS-pentacene) coated *p*-type graphene, it induces charge transfer and air-stable *n*-doping (Fig. 10(a)). By adjusting the irradiation time (or intensity), the Dirac point of a graphene FET gradually shifts from positive (*p*-type) to zero (intrinsic) then to negative (*n*-type) gate voltages (Fig. 10 (b)). This method only requires spin-coating of TIPS-pentacene and a low-power visible laser fabrication system. This method is facile and cost-effective, opening the door for fabricating cost-effective graphene electronics at large scales. The focused-laser inducing *p*-*n* junctions in graphene provide a promising route to build graphene-based electronics and optoelectronic devices. Furthermore, the fabrication method are also applicable to control the bandgap in other TMDCs materials [29].

3.1.5 Transparent conductive electrode

Transparent and flexible electronics have been of great interest due to their attractive applications in displays, touch panels and photovoltaics [60,61]. Kymakis et al. showed laser reduced GO films can be utilized as transparent electrodes in flexible, bulk heterojunction and organic photovoltaic (OPV) devices, potentially replacing the conventional indium tin oxide (ITO), as shown in Fig. 11 [61]. Figure 11(a) shows the sheet resistance (R_{SH}) and transmittance (T_R) at λ = 550 nm of laser reduced GO films of various thicknesses. Notably, both R_{SH} and T_R decreased with the increasing thickness of GO. The

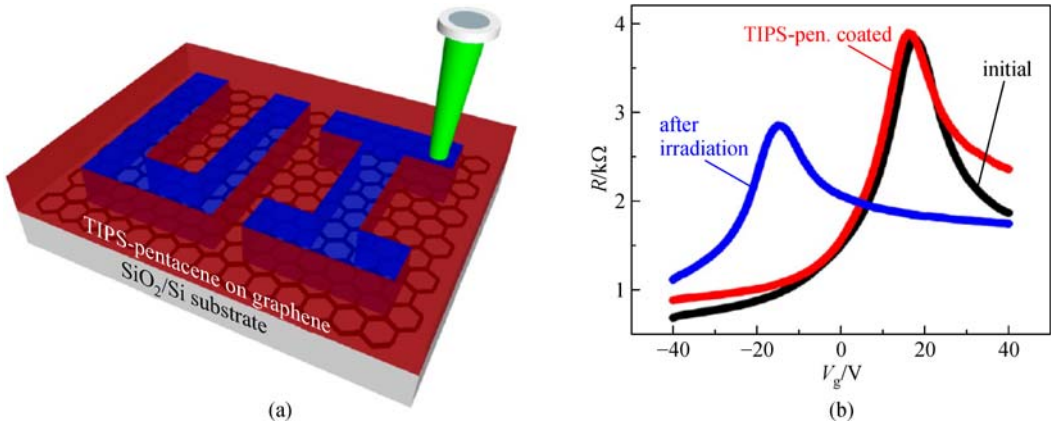

Fig. 10 (a) Fabricated n-doped regions in the form of the letters "UI" with the laser writing method; (b) resistance *vs* gate voltage (R-V_g) curves for a graphene FET as fabricated (black line), after spin coating TIPS-pentacene (red line), and after laser irradiation of the entire channel area (blue line) [59]

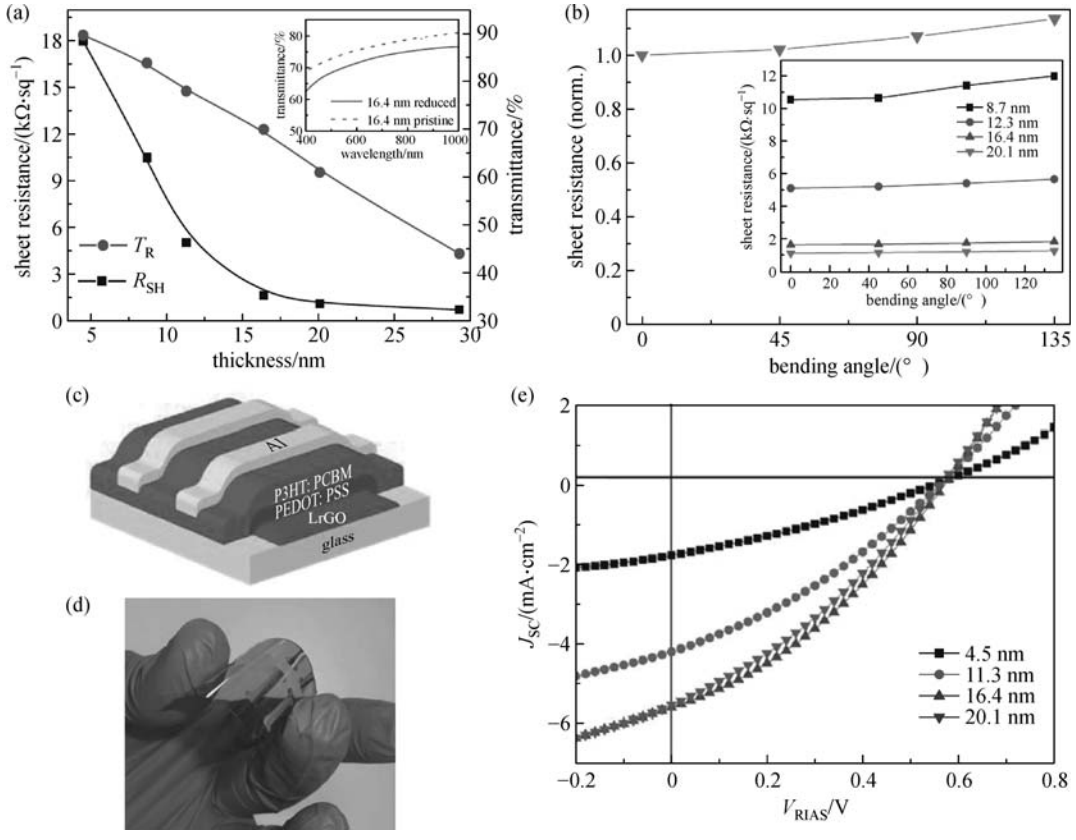

Fig. 11 (a) Transmittance at 550 nm and sheet resistance of the laser reduced GO (LrGO) films on PET substrates as a function of their film thickness. The inset shows the UV-vis transmittance spectra of the LrGO films on PET; (b) sheet resistance (normalized to the unbending sheet resistance) for various bending angles and thicknesses; (c) schematic and (d) picture of the flexible PET/r-GO/PEDOT: PSS/P3HT:PCBM/Al photovoltaic devices fabricated; (e) illuminated current-voltage (J-V) curves of the solar cells with various LrGO film thicknesses [61]

obtained lowest R_{SH} is 0.7 kΩ/sq for the 20.1 nm thick laser reduced GO film whose transmittance is 44%. The highest optical transparency of 88% was obtained for the 4.5 nm thick laser reduced GO, but the R_{SH} is 18 kΩ/sq. The flexible electronics technology requires electrodes exhibiting simultaneous high transparency and conductivity complemented by flexibility. Figure 11(b) depicts the averaged R_{SH} of the laser reduced GO films with various

thicknesses, normalized with the R_{SH} before bending, under different bending angles. It is observed that the electrical characteristics of the flexible laser reduced GO films show no significant dependence on the bending angle. Figure 11(e) presents the illuminated *J-V* characteristics of the OPV devices with laser reduced GO thickness of 4.6, 11.3, 16.4 and 20.1 nm. The optimum thickness is about 16.4 nm, where a J_{SC} of 5.62 mA/cm^2, a V_{OC} of 0.57 V and an overall power-conversion efficiency of 1.1% is obtained, which is the highest reported result for OPV device incorporating reduced GO as the transparent electrode so far. The *in situ* photo-reduction of GO films creates a new way to produce flexible functional graphene electrodes for various electronic applications in a process that carries substantial promise for industrial implementation [61].

3.1.6 Laser-induced microstructuring of 2D perovskite

Recently, organic-inorganic hybrid materials have become a hot topic toward optoelectronic applications. Metal halide lead perovskites, depending on the chemical interaction between organic and inorganic entities, showing a wide range of crystal packing and diverse properties. The applications of 2D organic-inorganic perovskites in photonic devices were studied by embedding them into micro-cavities, waveguides, distributed Bragg reflectors and patterned metallic/dielectric gratings using complicated fabrication protocols [62–64].

Among various patterning methods, DLW as a facile and non-contact method stands out and has been utilized to pattern various organic (polymers and sol-gel materials) and inorganic (silicon) materials. However, both organic and inorganic entities are together in perovskites, hence optimisation of patterning could be a formidable task due to the insufficient information on laser induced chemical/physical effects of these hybrid materials. In this regard, Kanaujia et al. reported the laser interaction of 2D perovskite thin films, which explained concurrent changes in the morphological and optical properties of 2D perovskites during the DLW process [65]. The occurrence of laser interaction in these systems is due to a single photon absorption related mechanism, as shown in Fig. 12 (a). During the laser-material interaction, the imparted

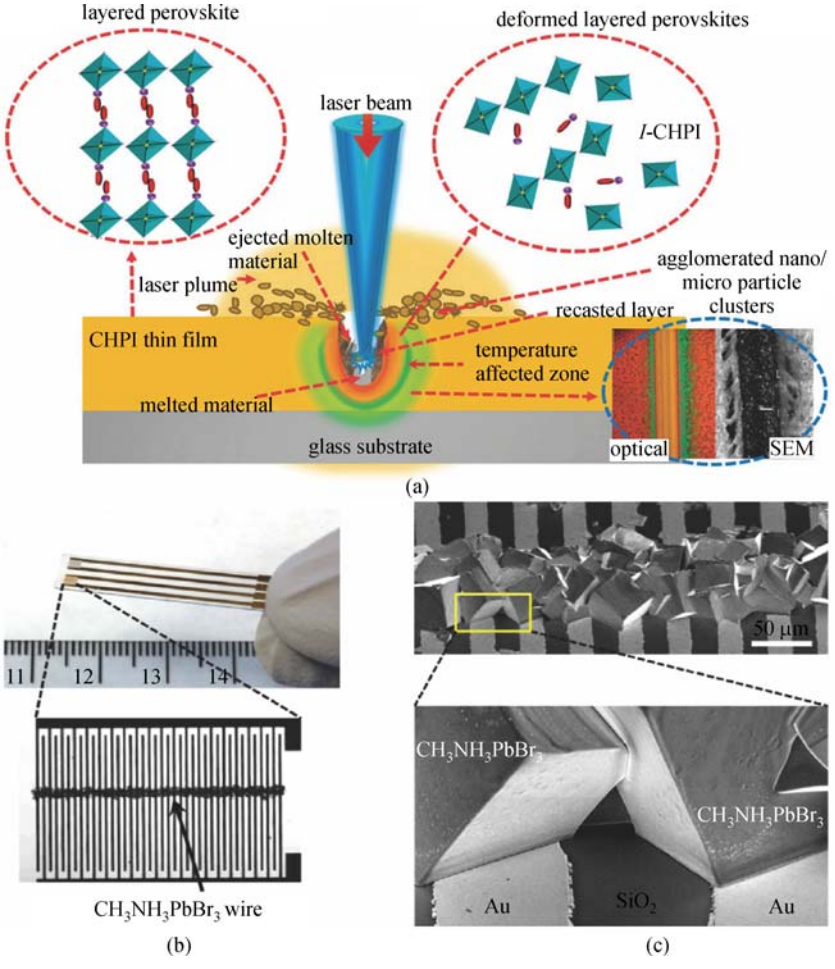

Fig. 12 (a) Schematic of the laser-material interaction mechanism of organic-inorganic perovskite laser writing; (b) direct laser writing $CH_3NH_3PbBr_3$ wire drawn onto an Au interdigitated microelectrode; (c) SEM of the $CH_3NH_3PbBr_3$ wire [65,66]

energy diffuses into the surrounding area. Due to a relatively high power density at the laser focus spot, the local temperature of the interaction zone increases, which is known as the temperature affected zone. Once the material starts melting and consequently the material evaporation takes place, forming a plasma plume which consists of evaporated hot organic-inorganic perovskite nanoparticles. Due to gravitational pull and temperature gradients, these hot nanoparticles release heat and start condensing at the nearby edge area [65].

Chou et al. showed DLW of lead halide perovskites, a facile method that takes advantage of the inverse dependence between perovskite solubility and temperature via laser to induce localized heating of an absorbing substrate [66]. They showed arbitrary pattern formation of crystalline $CH_3NH_3PbBr_3$ on various substrates, and then fabricated and characterized a microscale photodetector, as shown in Figs. 12(b) and 12(c). This DLW method provides a path toward the prototyping and production of perovskite-based devices. It was showed lead perovskite precursors exhibit an inverse relationship between solubility and temperature. This relationship provides a simple mechanism to spatially confine crystal growth, e.g., using a laser to induce microscale heating of a transducing substrate. Indeed, this premise turns out to be straightforward, and allows for the advancement of DLW of lead halide perovskites materials routinely from bath solution. This method provides site-specific integration of perovskite functionality onto platforms used in electronics via fabrication of a microscale photodetector incorporating a perovskite wire.

In summary, all the above examples show DLW can be well used to fabricate 2D material functional devices with unique performance properties not achievable before. These include ultrathin flat lens, ultrathin polarizes, perfect absorbers, *p-n* junctions, transport conductive electrode and etc., which demonstrate the flexibility and cost-effective properties of DLW technique. Furthermore, DLW has been used to locally change the nonlinear properties (nonlinear absorption coefficient and nonlinear refractive index) of GO materials, which offers a new flexibility in modifying the device performance for all-optical communication devices [67–69].

3.2 Electrochemical energy storage

With the increasing demand of portable electronics, supercapacitors have attracted much attention due to their high power density, fast charge-discharge rate and superior cycling stability [70–75]. Among all the electrochemical energy storage devices, the flexible and miniaturized supercapacitors compatible with integrated energy storage devices have been explored and fabricated. Compared with the conventional heavy and bulky supercapacitors, the micro-supercapacitors are easily fabricated into various shapes and arrays via a facile design and integration, making them promising for stand-alone power sources for microelectronics devices. Graphene is a promising electrode material due to its prominent advantages of large specific surface area (SSA), mechanical strength, and electrical properties. GO has been widely used in different charge-storage devices. However, compared with the theoretical value of a monolayer of graphene, the specific capacitance, energy density, and power density of GO-based devices are still low because of the van der Waals interaction induced restacking of RGO sheets during reduction, which largely reduces the SSA of RGO and leads to a relative low capacitance.

Due to its local-area material processing and high spatial resolution properties, laser-induced graphene-based materials with specific micro/nano-structures can offer great technological advances for micro-supercapacitors with ultrahigh power density. In this regard, El-Kady et al. proposed a strategy for graphene-based supercapacitors via a standard LightScribe DVD optical drive to conduct laser reduction of GO to laser-scribed graphene (LSG) [76]. Such method could efficiently prevent the restacking of graphene sheets and enable the LSG with high mechanical robustness to reach a high SSA of 1520 m^2/g and excellent conductivity of 1738 S/m (Fig. 13(a)). Ultrathin (thickness < 100 μm) supercapacitor was fabricated without any binder or current collectors, which showed ultrahigh energy density values (1.36 mWh/cm^3) in different electrolytes, approximately two times higher than that of a commercial activated-carbon supercapacitors, making it potentially useful in micro-device applications. Subsequently, this group further achieved the direct light scribe of interdigitated graphene micro-supercapacitors on the disc based on a computer-designed circuit by using LightScribe DVD burner (Fig. 13(b)) [77]. This in-plane patterned LSG showed a much high conductivity of 2350 S/m and could be directly applied in micro-supercapacitors after adding the electrolyte. Compared with conventional micro-fabrication strategies, this efficient method facilitated the construction of micro-devices with high area density, in which more than 100 micro-supercapacitors could be produce on a DVD disc with a lateral spatial resolution of ~ 20 μm (Figs. 13(c) and 13(d)). These fabricated electrodes reached a high power density of 200 W/cm^3, and even maintained 96% of their initial performance after 10000 consecutive charge-discharge cycles. The devices are built on flexible substrates for flexible electronics that can be integrated with microelectromechanical system (MEMS) or complementary metal oxide semiconductor (CMOS) in a single chip. However, light scribe is not adjustable and based on dot-by-dot fabrication, therefore it is limited to control the laser parameters.

Using a similar DLW method, all-carbon monolithic micro-supercapacitos on hydrated and self-supported GO film were constructed in-plane and conventional sandwiched structures with different geometries in RGO-GO-

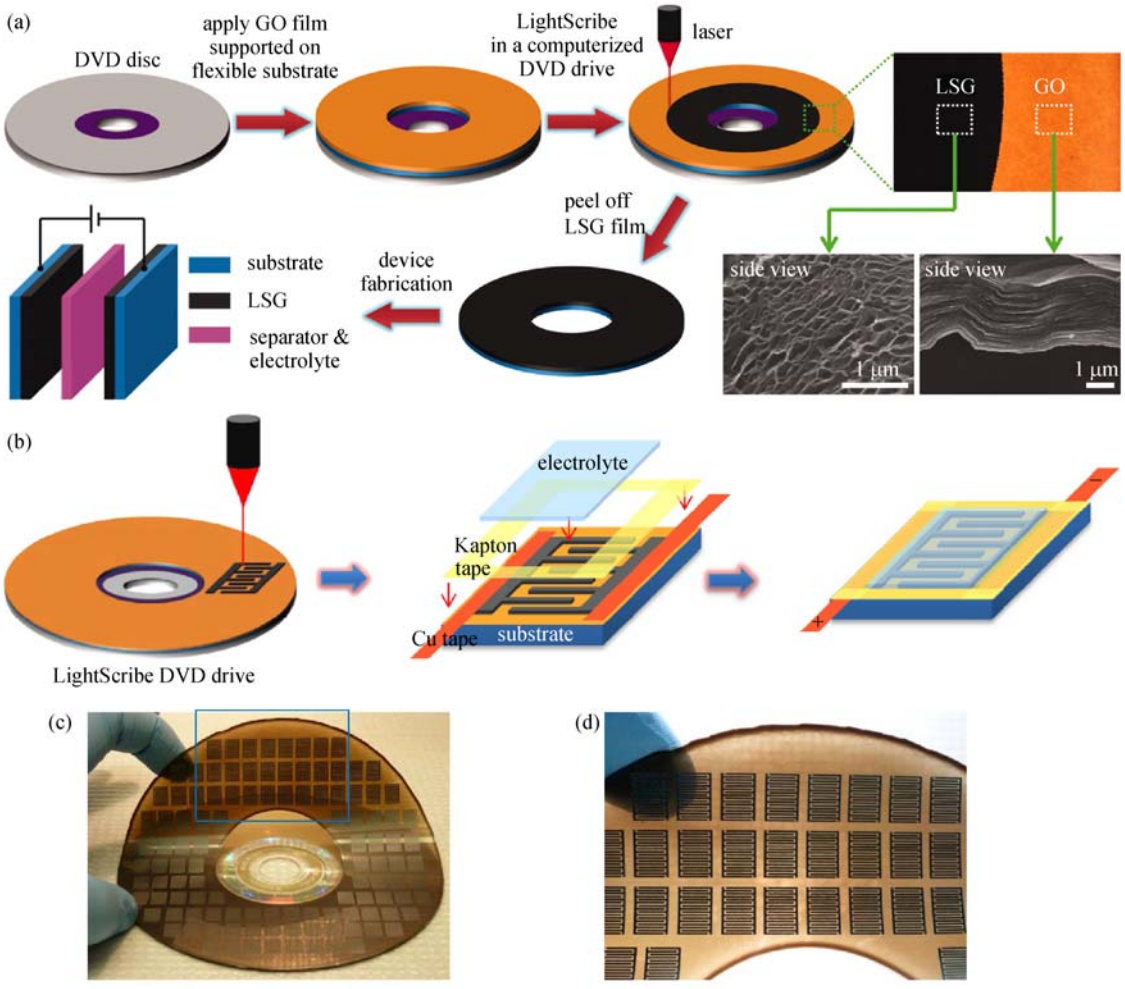

Fig. 13 (a) Fabrication process of laser-scribed graphene-based electrochemical capacitors; (b) schematic diagram of the preparation process for an LSG micro-supercapacitor; (c) and (d) photographs of 100 micro-devices on a single run with high flexibility [76,77]

RGO configurations via CO_2 DLW technique by Gao et al., as shown in Fig. 14(a) [78]. Selective ultrasonic removal of RGO or GO was realized through a precise control over the laser power and temperature of the substrate. Interestingly, as an ionic conductor and electrical insulator, the remaining hydrated GO area between patterned RGO electrodes could serve as an electrolyte as well as electrode separator due to the presence of trapped water with ion transport characteristics in the micro-supercapacitors. Figure 14(b) shows a photograph of an array of concentric circular RGO patterns fabricated on a free-standing hydrated GO film. The laser irradiation would induce the decomposition of functional groups and generate water vapor to release gases, leading to the porous structure of laser-reduced RGO region, as shown in Fig. 14(c). Consequently, the resulting micro-supercapacitor devices showed good cyclic stability and energy storage capacities. Especially, the in-plane circular patterned supercapacitor had the much high capacitance of 0.51 mF/cm^2 with a power density of 1.7 W/cm^3.

3.3 Other applications

3.3.1 Surface enhanced Raman scattering

Surface enhanced Raman scattering (SERS) is an attractive topic because it provides the fingerprints information on targeted molecules with high sensitivities, which shows a great potential in biomedical applications. To realize effective SERS measurements, it is crucial to design effective plasmonic structures as SERS substrates, which can enhance the Raman signal via localized surface plasmon resonance (LSPR) [79]. Using conventional micro/nano-fabrication methods, various kinds of metallic micro/nanostructures (e.g., close-packed metallic nanoparticles and multi-branched metallic nanocrystals) were designed for SERS measurements. However, these methods are complicated, which limits the practical applications. To realize a facile preparation of SERS substrates, rough metal surface have also been prepared by coating noble metal (e.g., gold and silver) nanoparticles on rough

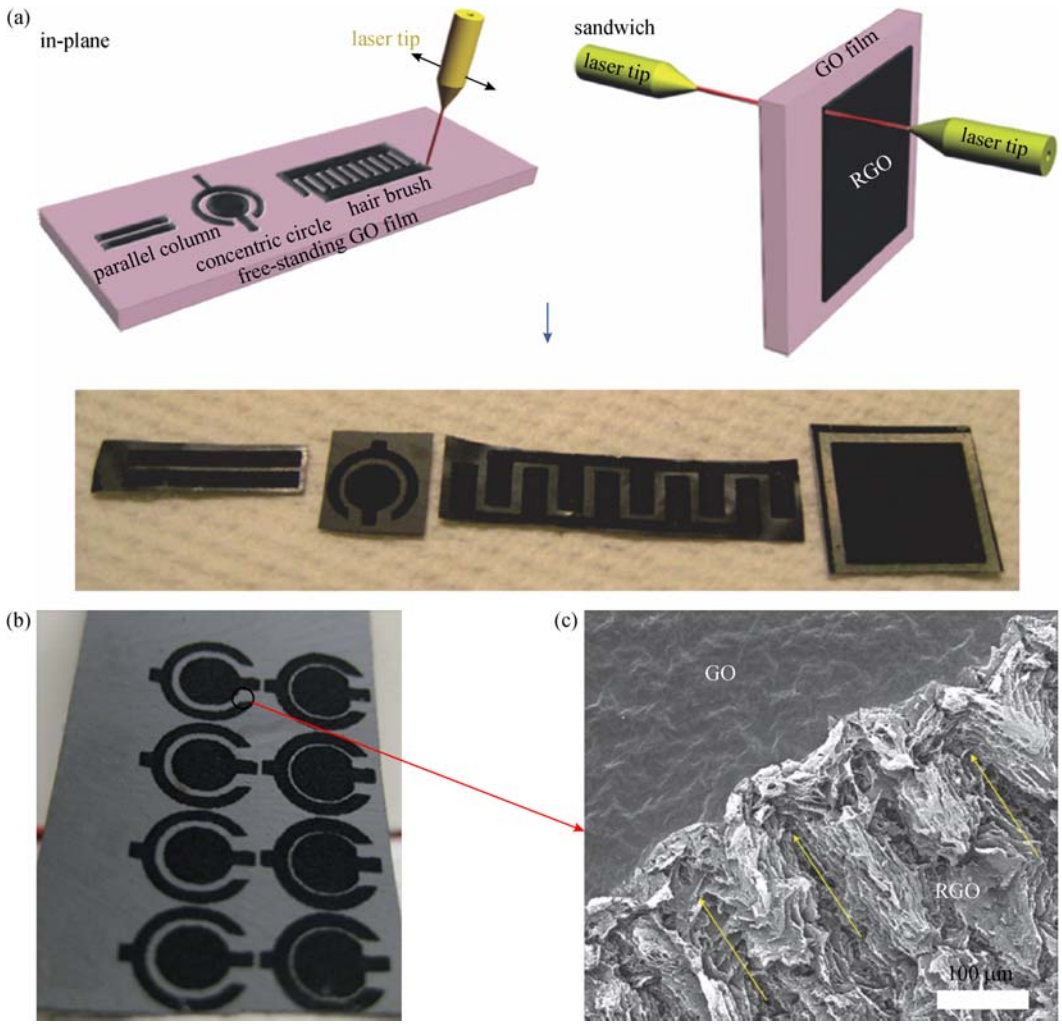

Fig. 14 (a) Schematics of CO_2 laser-patterning of free-standing hydrated GO films to fabricate RGO-GO-RGO devices with in-plane and sandwich geometries. The black contrast in the top schematics corresponds to RGO, and the light contrast to unmodified hydrated GO. For in-plane devices, three different geometries were used, and the concentric circular pattern gives the highest capacitance density. The bottom row shows photographs of patterned films; (b) photograph of an array of concentric circular patterns fabricated on a free-standing hydrated GO film; (c) SEM image of the interface between GO and RGO, with yellow arrows indicating a long-range pseudo-ordered structure generated by laser-beam scanning [78]

templates. However, such rough templates usually possess strong PL. Furthermore, both gold and silver films also have a strong PL background under laser excitation, which function as background noise, difficult for Raman signal collection. In this regard, graphene and its derivatives seem to be another suitable template for SERS since the extraordinary electronic properties may well address the above-mentioned concerns by effectively quenching the fluorescence signal from the probe molecules. In addition, graphene derivatives show additional chemical enhancing ability, high adsorption to target molecules, good biocompatibility and anti-oxidation of silver nanoparticels (AgNPs), which are highly beneficial for SERS signals. Thus, rational combination of GO/RGO and noble metal nanoparticles could largely improve the SERS performance.

Yan et al. reported the fabrication of RGO grating structures by TBLI for highly efficient SERS substrates via simple physical vapor deposition coating of silver, as shown in Fig. 15(a) [79]. TBLI has been used to fabricate hierarchical RGO grating structures with microscale gratings and nanoscale folders through a laser induced ablation and photo-reduction process (Fig. 5). The hierarchical structures contribute to the formation of plasmonic structures after AgNPs coating, giving rise to the formation of many SERS “hot spots,” while the RGO substrate would provide chemical enhancement of Raman signal through interaction with target molecules. The significantly increased roughness with respect to the hierarchical structures in combination with the removal of hydrophilic oxygen-containing groups endows the resultant substrates with unique super-hydrophobicity,

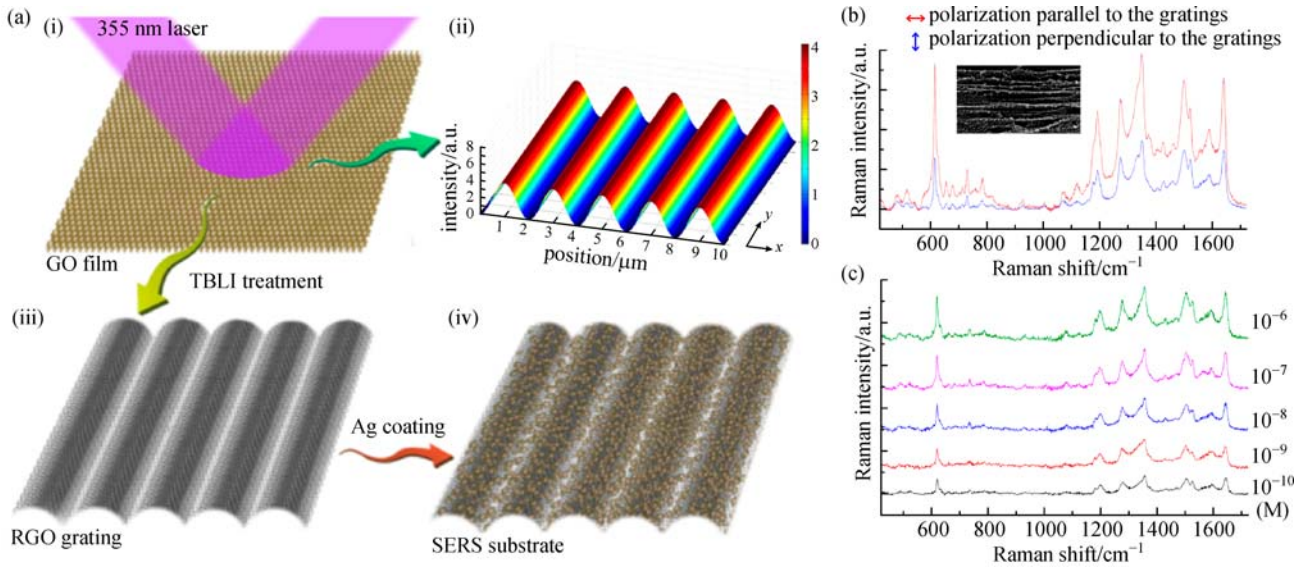

Fig. 15 (a) Schematic illustration of TBLI fabrication of RGO gratings and subsequent silver coating toward the development of SERS substrates. (i) TBLI treatment of GO film; (ii) light intensity distribution of two interfered laser beams; (iii) RGO gratings; and (iv) Ag-RGO gratings as SERS substrates; (b) comparison of SERS measured with two different laser polarization directions with respect to the gratings, red and blue curves show the SERS spectra measured with the polarization parallel and perpendicular to the gratings, respectively. (Inset) SEM image of the Ag-RGO gratings; red and blue marks show the laser polarization directions; (c) SERS spectra of RhB solution with different concentrations, from top to bottom the concentration decreased from 10^{-6} to 10^{-10} M [79]

which leads to the enhancement of analytes and further increases the detection sensitivity. The synergistic effects make the silver-coated RGO (Ag-RGO) gratings as a highly efficient SERS substrate. It showed high SERS enhancement, low detection limit (10^{-10} M) and high reproducibility in the test of rhodamine B (RhB), as shown in Figs. 15(b) and 15(c). As a rapid, mask-free, chemical-free, and flexible laser processing technology, TBLI has great potential for making RGO micro/nano-structures toward the development of SERS substrates.

Furthermore, the focused laser beam has been proved to enable selective self-assembly of gold nanoparticles (AuNPs) on the surface of a MoS_2 film to form functional hybrids. Considering the strong coupling of AuNPs to the Raman signal and the efficient adsorption of aromatic organic molecules on the MoS_2, the as-prepared AuNPs-MoS_2 hybrid can conduct as superior SERS substrates for the detection of aromatic organic molecules. These SERS substrates present a sensitive detection ability to molecules of methylene blue and rhodamine 6G even at the resonance excitation wavelength. With the extensive applicability of the laser techniques, DLW is expected to play a significant role in extending the functionalities of a broad range of 2D materials [30].

3.3.2 Biomedical applications

The attractive properties of graphene and its derivatives for biomedical applications have been explored as versatile platforms to promote neural cell alignment and cell differentiation processes [80–84]. Using DLW approach, Lorenzoni et al. fabricated patterned graphene substrates that promoted ordered growth of primary embryonic hippocampal neurons, as shown in Fig. 16 [83]. Chemical vapor deposition single layer graphene was fabricated by single pulse UV laser ablation at the lowest effective laser power. Patterned substrates were then coated with poly-D-lysine by means of a simple immersion in solution (Fig. 16 (a)). The functionalization is more effective on the single layer graphene, resulting in notably higher alignment for neuron adhesion and growth (Figs. 16(b) and 16(c)). Peláez et al. used laser interferometry to generate fringed channels with topography on partially RGO layers (thickness of (12±4) nm) as a substrate, then studied cell adhesion, morphology, viability, and differentiation in embryonic neural progenitor cells on platforms with a period of 9.4 μm (higher than the typical dimensions of neural somas) [84]. Fringed platforms significantly promote neurite alignment (~50% at 6 d), while preserving viability and neural differentiation. The laser-based method promise a meaningful tool for the advanced neural interfaces, such as electrodes and biosensors, either by patterning bulk materials or as fringed graphene-based coatings of pre-existing ones [84].

Moreover, BP nanosheets have been proved to have great possibility to enable efficient loading of theranostic agents, similar to graphene, MoS_2, because of the atomically thin 2D structure and relatively large surface area. Tao et al. revealed the biological activities and screened the endocytosis pathways of PEGylated BP nanosheets in

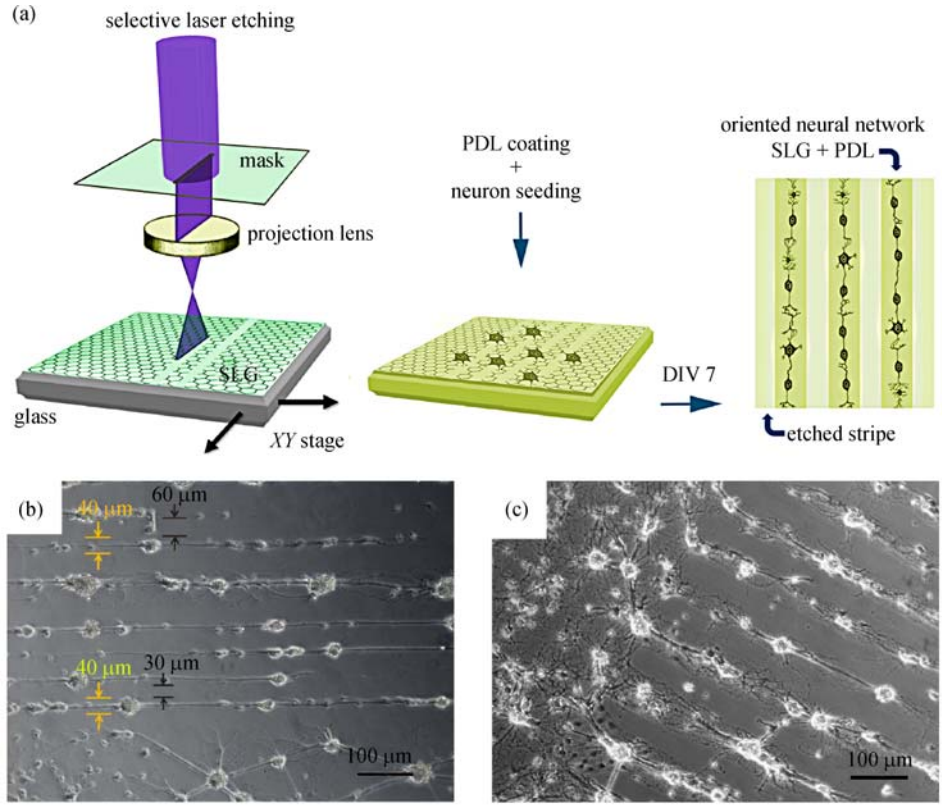

Fig. 16 (a) Schematics of the steps proposed to create an ordered neural network on single layer graphene (SLG) substrate; (b) and (c) neural networks oriented along line patterns. In (b) yellow markers indicate the width of graphene stripes, kept at 40 μm, black markers indicate the width of etched stripes, i.e., 30 and 60 μm in the pattern shown. In (c) the boundary region between graphene (upper left) and patterned graphene is shown. For the samples shown the fluency used during laser patterning was 0.8 J/cm^2 [83]

cancer cells, providing guidance for the essential understanding of BP and other emerging 2D nanomaterials for cancer theranostics [85]. Both *in vitro* and *in vivo* experiments verified the safety and enhanced antitumor effect. The black phosphorus quantum dots (BPQDs) also exhibited an excellent near infrared (NIR) photo-thermal performance and good photostability [86,87]. After PEG conjugation, the BPQDs showed enhanced stability in physiologic medium, and there was no toxicity to different types of cells. NIR photoexcitation of the BPQDs led to significant cell death, suggesting that the nanoparticles have large potential as photo-thermal agents.

4 Conclusions

Employing direct laser fabrication technique to achieve complex micro/nano-structures of 2D materials has attracted numerous interests. It has been widely studied for broad applications in the integrated photonics and optoelectronics, electrochemical energy storage and etc. In this review, we have summarized the design and fabrication of 2D materials through laser processing, including direct patterning, controllable thinning, doping and functionalization, along with the recent progress in applying these integrated materials in photonics and optoelectronics devices, electrochemical energy storage devise, sensing and biomedical applications.

The direct laser fabrication method forms a promising strategy for simple, rapid and large-scale fabrication of various patterns without masks and harsh conditions. Ultrafast lasers can drive a wide range of subtractive and additive processes for the patterning and functionalization of 2D materials. Mechanisms such as multiphoton absorption, thermal effects, non-thermal interactions, photochemical effects, as well as compatibility and integration with advanced diagnostics can be beneficial in this effort. Furthermore, ultrafast lasers can be used for scalable processing and therefore realize the next-generation high-performance portable, integratable and flexible devices based on 2D materials. Depending on the repetition rate of the ultrafast laser, the thermal effect can be minimized in the fabrication process. In contrast, CW laser fabrication is mainly a thermal based effect. The absorbed laser energy is rapidly converted into local heat and raises the local temperature, leading to the structural change and fabrication of materials. The laser wavelength also plays a significant role in the laser fabrication. The wavelength falls within the absorption band of the materials can enable single photon fabrication efficiently.

When the illumination wavelength is beyond the single photon absorption band, a tightly focused pulsed laser beam is required to enable two-photon based nonlinear absorption.

Further advancements rely on both super-resolution [88] and parallel writing method (multifocal direct laser printing) [89] to achieve better selectivity and molecular level manipulation with high productivity. Combining this versatile DLW technique with the super-resolution and parallel writing method, it is promising to lead to a novel laser-based fabrication platform enabling multidimensional functional and scalable 2D material fabrication. With the joint efforts from material science, laser engineering and device process design showing up, promises innovative solutions to grand challenges, which were difficult to solve before.

Acknowledgements Baohua Jia acknowledges the support from the Australia Research Council through the Discovery Project scheme (DP150102972) and the support from Defense Science Institute and Defense Science and Technology Group.

References

1. Zhang H. Ultrathin two-dimensional nanomaterials. ACS Nano, 2015, 9(10): 9451–9469
2. Ponraj J S, Xu Z Q, Dhanabalan S C, Mu H, Wang Y, Yuan J, Li P, Thakur S, Ashrafi M, Mccoubrey K, Zhang Y, Li S, Zhang H, Bao Q. Photonics and optoelectronics of two-dimensional materials beyond graphene. Nanotechnology, 2016, 27(46): 462001
3. Xia F N, Wang H, Xiao D, Dubey M, Ramasubramaniam A. Two-dimensional material nanophotonics. Nature Photonics, 2014, 8(12): 899–907
4. Brar V W, Koltonow A R, Huang J X. New discoveries and opportunities from two-dimensional Materials. ACS Photonics, 2017, 4(3): 407–411
5. Novoselov K S, Fal′ko V I, Colombo L, Gellert P R, Schwab M G, Kim K. A roadmap for graphene. Nature, 2012, 490(7419): 192–200
6. Zhang Y B, Rubio A, Lay G L. Emergent elemental two-dimensional materials beyond graphene. Journal of Physics. D, Applied Physics, 2017, 50(5): 053004
7. Bhimanapati G R, Lin Z, Meunier V, Jung Y, Cha J, Das S, Xiao D, Son Y, Strano M S, Cooper V R, Liang L, Louie S G, Ringe E, Zhou W, Kim S S, Naik R R, Sumpter B G, Terrones H, Xia F, Wang Y, Zhu J, Akinwande D, Alem N, Schuller J A, Schaak R E, Terrones M, Robinson J A. Recent advances in two-dimensional materials beyond Graphene. ACS Nano, 2015, 9(12): 11509–11539
8. Geim A K. Graphene: status and prospects. Science, 2009, 324 (5934): 1530–1534
9. Bonaccorso F, Sun Z P, Hasan T, Ferrari A C. Graphene photonics and optoelectronics. Nature Photonics, 2010, 4(9): 611–622
10. Mak K F, Shan J. Photonics and optoelectronics of 2D semiconductor transition metal dichalcogenides. Nature Photonics, 2016, 10(4): 216–226
11. Xia F, Wang H, Jia Y. Rediscovering black phosphorus as an anisotropic layered material for optoelectronics and electronics. Nature Communications, 2014, 5: 4458
12. Castellanos-Gomez A. Black phosphorus: Narrow gap, wide applications. The Journal of Physical Chemistry Letters, 2015, 6 (21): 4280–4291
13. Dou L, Wong A B, Yu Y, Lai M, Kornienko N, Eaton S W, Fu A, Bischak C G, Ma J, Ding T, Ginsberg N S, Wang L W, Alivisatos A P, Yang P. Atomically thin two-dimensional organic-inorganic hybrid perovskites. Science, 2015, 349(6255): 1518–1521
14. Huo C X, Cai B, Yuan Z, Ma B W, Zeng H B. Two-dimensional metal halide perovskites: theory, synthesis, and optoelectronics. Small Methods, 2017, 1(3): 1600018
15. Chen S, Shi G. Two-dimensional materials for halide perovskite-based optoelectronic devices. Advanced Materials, 2017, 29(24): 1605448
16. Choi D G, Jeong J H, Sim Y S, Lee E S, Kim W S, Bae B S. Fluorinated organic-inorganic hybrid mold as a new stamp for nanoimprint and soft lithography. Langmuir, 2005, 21(21): 9390–9392
17. Pardo D A, Jabbour G E, Peyghambarian N. Application of screen printing in the fabrication of organic light-emitting devices. Advanced Materials, 2000, 12(17): 1249–1252
18. Caruso F. Hollow capsule processing through colloidal templating and self-assembly. Chemistry (Weinheim an der Bergstrasse, Germany), 2000, 6(3): 413–419
19. Zhang J C, Zhou M J, Wu W D, Tang Y J. Fabrication of diamond microstructures by using dry and wet etching methods. Plasma Science & Technology, 2013, 15(6): 552–554
20. Zhang Y L, Guo L, Wei S, He Y Y, Xia H, Chen Q D, Sun H B, Xiao F S. Direct imprinting of microcircuits on graphene oxides film by femtosecond laser reduction. Nano Today, 2010, 5(1): 15–20
21. Zhang Y L, Chen Q D, Xia H, Sun H B. Designable 3D nanofabrication by femtosecond laser direct writing. Nano Today, 2010, 5(5): 435–448
22. Zheng X R, Lin H, Yang T S, Jia B H. Laser trimming of graphene oxide for functional photonic applications. Journal of Physics D, Applied Physics, 2017, 50(7): 074003
23. Yu S, Wu X, Wang Y, Guo X, Tong L. 2D materials for optical modulation: challenges and opportunities. Advanced Materials, 2017, 29(14): 1606128
24. Sun Z P, Martinez A, Wang F. Optical modulators with 2D layered materials. Nature Photonics, 2016, 10(4): 227–238
25. Wang F Q. Two-dimensional materials for ultrafast lasers. Chinese Physics B, 2017, 26(3): 034202
26. Yoo J H, Kim E, Hwang D J. Femtosecond laser patterning, synthesis, defect formation, and structural modification of atomic layered materials. MRS Bulletin, 2016, 41(12): 1002–1008
27. Li Z W, Hu Y H, Li Y, Fang Z Y. Light-matter interaction of 2D materials: physics and device applications. Chinese Physics B, 2017, 26(3): 036802
28. Ye M X, Zhang D Y, Yap Y K. Recent advances in electronic and optoelectronic devices based on two-dimensional transition metal dichalcogenides. Electronics (Basel), 2017, 6(2): 43
29. Zhao Y, Han Q, Cheng Z H, Jiang L, Qu L T. Integrated graphene systems by laser irradiation for advanced devices. Nano Today, 2017, 12: 14–30
30. Lu J, Liu H, Tok E S, Sow C H. Interactions between lasers and two-

dimensional transition metal dichalcogenides. Chemical Society Reviews, 2016, 45(9): 2494–2515

31. Xiong W, Zhou Y S, Hou W J, Jiang L J, Mahjouri-Samani M, Park J, He X N, Gao Y, Fan L S, Baldacchini T, Silvanin J F, Lu Y F. Laser-based micro/nanofabrication in one, two and three dimensions. Frontiers of Optoelectronics, 2015, 8(4): 351–378
32. Xiong W, Zhou Y S, Hou W J, Jiang L J, Gao Y, Fan L S, Jiang L, Silvain J F, Lu Y F. Direct writing of graphene patterns on insulating substrates under ambient conditions. Scientific Reports, 2014, 4(1): 4892
33. Zhang Y L, Guo L, Xia H, Chen Q D, Feng J, Sun H B. Photoreduction of graphene oxides: methods, properties, and applications. Advanced Optical Materials, 2014, 2(1): 10–28
34. Cote L J, Cruz-Silva R, Huang J. Flash reduction and patterning of graphite oxide and its polymer composite. Journal of the American Chemical Society, 2009, 131(31): 11027–11032
35. Gilje S, Dubin S, Badakhshan A, Farrar J, Danczyk S A, Kaner R B. Photothermal deoxygenation of graphene oxide for patterning and distributed ignition applications. Advanced Materials, 2010, 22(3): 419–423
36. Koinuma M, Ogata C, Kamei Y, Hatakeyama K, Tateishi H, Watanabe Y, Taniguchi T, Gezuhara K, Hayami S, Funatsu A, Sakata M, Kuwahara Y, Kurihara S, Matsumoto Y. Photochemical engineering of graphene oxide nanosheets. Journal of Physical Chemistry C, 2012, 116(37): 19822–19827
37. Li X H, Chen J S, Wang X, Schuster M E, Schlögl R, Antonietti M. A green chemistry of graphene: photochemical reduction towards monolayer graphene sheets and the role of water adlayers. ChemSusChem, 2012, 5(4): 642–646
38. Stroyuk A L, Andryushina N S, Shcherban' N D, Il'in V G, Efanov V S, Yanchuk I B, Kuchmii S Y, Pokhodenko V D. Photochemical reduction of graphene oxide in colloidal solution. Theoretical and Experimental Chemistry, 2012, 48(1): 2–13
39. Castellanos-Gomez A, Barkelid M, Goossens A M, Calado V E, van der Zant H S J, Steele G A. Laser-thinning of MoS_2: on demand generation of a single-layer semiconductor. Nano Letters, 2012, 12 (6): 3187–3192
40. Han G H, Chae S J, Kim E S, Güneş F, Lee I H, Lee S W, Lee S Y, Lim S C, Jeong H K, Jeong M S, Lee Y H. Laser thinning for monolayer graphene formation: heat sink and interference effect. ACS Nano, 2011, 5(1): 263–268
41. Lu J, Carvalho A, Chan X K, Liu H, Liu B, Tok E S, Loh K P, Castro Neto A H, Sow C H. Atomic healing of defects in transition metal dichalcogenides. Nano Letters, 2015, 15(5): 3524–3532
42. Cho S, Kim S, Kim J H, Zhao J, Seok J, Keum D H, Baik J, Choe D H, Chang K J, Suenaga K, Kim S W, Lee Y H, Yang H. Phase patterning for ohmic homojunction contact in $MoTe_2$. Science, 2015, 349(6248): 625–628
43. Lu J, Wu J, Carvalho A, Ziletti A, Liu H, Tan J, Chen Y, Castro Neto A H, Özyilmaz B, Sow C H. Bandgap engineering of phosphorene by laser oxidation toward functional 2D materials. ACS Nano, 2015, 9(10): 10411–10421
44. Guo L, Zhang Y L, Han D D, Jiang H B, Wang D, Li X B, Xia H, Feng J, Chen Q D, Sun H B. Laser‐mediated programmable N doping and simultaneous reduction of graphene oxides. Advanced Optical Materials, 2014, 2(2): 120–125
45. Savva K, Lin Y H, Petridis C, Kymakis E, Anthopoulos T D, Stratakis E. In situ photo-induced chemical doping of solution-processed graphene oxide for electronic applications. Journal of Materials Chemistry C, Materials for Optical and Electronic Devices, 2014, 2(29): 5931–5937
46. Kim E, Ko C, Kim K, Chen Y, Suh J, Ryu S G, Wu K, Meng X, Suslu A, Tongay S, Wu J, Grigoropoulos C P. Site selective doping of ultrathin metal dichalcogenides by laser‐sssisted reaction. Advanced Materials, 2016, 28(2): 341–346
47. Zhang Y L, Xia H, Kim E, Sun H B. Recent developments in superhydrophobic surfaces with unique structural and functional properties. Soft Matter, 2012, 8(44): 11217–11231
48. Jiang H B, Zhang Y L, Han D D, Xia H, Feng J, Chen Q D, Hong Z R, Sun H B. Bioinspired fabrication of superhydrophobic graphene films by two-beam laser interference. Advanced Functional Materials, 2014, 24(29): 4595–4602
49. Xie Q, Hong M H, Tan H L, Chen G X, Shi L P, Chong T C. Fabrication of nanostructures with laser interference lithography. Journal of Alloys and Compounds, 2008, 449(1-2): 261–264
50. Zheng X, Jia B, Lin H, Qiu L, Li D, Gu M. Highly efficient and ultra-broadband graphene oxide ultrathin lenses with three-dimensional subwavelength focusing. Nature Communications, 2015, 6: 8433
51. Lin H, Xu Z Q, Bao Q L, Jia B H. Laser fabricated ultrathin flat lens in sub-nanometer thick monolayer transition metal dichalcogenides crystal. In: Proceedings of Conference on Lasers and Electro-Optics (CLEO), 2016, SF2E.4, 1–2
52. Yu N, Capasso F. Flat optics with designer metasurfaces. Nature Materials, 2014, 13(2): 139–150
53. Zheng X R. The optics and applications of graphene oxide. Dissertation for the Doctoral Degree. Australia: Swinburne University of Technology, 2016
54. Zheng X R, Cao Z, Jia B H, Qiu L, Li D, Gu M. Direct patterning of C-shape arrays on graphene oxide thin films using direct laser printing. In: Proceedings of Frontiers in Optics 2014. Tucson, Arizona: Optical Society of America, FW2B
55. Bao Q L, Zhang H, Wang B, Ni Z H, Lim C H Y X, Wang Y, Tang D Y, Loh K P. Broadband graphene polarizer. Nature Photonics, 2011, 5(7): 411–415
56. Jia B H, Zheng X R, Lin H, Yang Y Y, Fraser S. Graphene oxide thin films for functional photonic devices. In: Proceedings of Frontiers in Optics 2016. Rochester, New York: Optical Society of America, FTu5B.4
57. Kim Y D, Bae M H, Seo J T, Kim Y S, Kim H, Lee J H, Ahn J R, Lee S W, Chun S H, Park Y D. Focused-laser-enabled p-n junctions in graphene field-effect transistors. ACS Nano, 2013, 7(7): 5850–5857
58. El-Kady M F, Kaner R B. Direct laser writing of graphene electronics. ACS Nano, 2014, 8(9): 8725–8729
59. Seo B H, Youn J, Shim M. Direct laser writing of air-stable p-n junctions in graphene. ACS Nano, 2014, 8(9): 8831–8836
60. Kymakis E, Petridis C, Anthopoulos T D, Stratakis E. Laser-assisted reduction of graphene oxide for flexible, large-area optoelectronics. IEEE Journal of Selected Topics in Quantum Electronics, 2014, 20 (1): 106–115
61. Kymakis E, Savva K, Stylianakis M M, Fotakis C, Stratakis E.

Flexible organic photovoltaic cells with *in situ* nonthermal photoreduction of spin-coated graphene oxide electrodes. Advanced Functional Materials, 2013, 23(21): 2742–2749
62. Cao D H, Stoumpos C C, Farha O K, Hupp J T, Kanatzidis M G. 2D homologous perovskites as light-absorbing materials for solar cell applications. Journal of the American Chemical Society, 2015, 137 (24): 7843–7850
63. Tsai H, Nie W, Blancon J C, Stoumpos C C, Asadpour R, Harutyunyan B, Neukirch A J, Verduzco R, Crochet J J, Tretiak S, Pedesseau L, Even J, Alam M A, Gupta G, Lou J, Ajayan P M, Bedzyk M J, Kanatzidis M G, Mohite A D. High-efficiency two-dimensional Ruddlesden-Popper perovskite solar cells. Nature, 2016, 536(7616): 312–316
64. Su R, Diederichs C, Wang J, Liew T C H, Zhao J, Liu S, Xu W, Chen Z, Xiong Q. Room temperature polariton lasing in all-inorganic perovskite nanoplatelets. Nano Letters, 2017, 17(6): 3982–3988
65. Kanaujia P K, Vijaya Prakash G. Laser-induced microstructuring of two-dimensional layered inorganic-organic perovskites. Physical Chemistry Chemical Physics, 2016, 18(14): 9666–9672
66. Chou S S, Swartzentruber B S, Janish M T, Meyer K C, Biedermann L B, Okur S, Burckel D B, Carter C B, Kaehr B. Laser direct write synthesis of lead halide perovskites. The Journal of Physical Chemistry Letters, 2016, 7(19): 3736–3741
67. Zheng X, Jia B, Chen X, Gu M. In situ third-order non-linear responses during laser reduction of graphene oxide thin films towards on-chip non-linear photonic devices. Advanced Materials, 2014, 26(17): 2699–2703
68. Fraser S, Zheng X R, Qiu L, Li D, Jia B H. Enhanced optical nonlinearities of hybrid graphene oxide films functionalized with gold nanoparticles. Applied Physics Letters, 2015, 107(3): 031112
69. Ren J, Zheng X R, Tian Z, Li D, Wang P, Jia B H. Giant third-order nonlinearity from low-loss electrochemical graphene oxide film with a high power stability. Applied Physics Letters, 2016, 109(22): 221105
70. Thangavelu P, Jong-Beom B.Graphene based 2D-materials for supercapacitors. 2D Materials, 2015, 2: 032002
71. Dong Y, Wu Z S, Ren W C, Cheng H M, Bao X H. Graphene: a promising 2D material for electrochemical energy storage. Science Bulletin, 2017, 62(10): 724–740
72. Shao Y, El-Kady M F, Wang L J, Zhang Q, Li Y, Wang H, Mousavi M F, Kaner R B. Graphene-based materials for flexible supercapacitors. Chemical Society Reviews, 2015, 44(11): 3639–3665
73. Raccichini R, Varzi A, Passerini S, Scrosati B. The role of graphene for electrochemical energy storage. Nature Materials, 2015, 14(3): 271–279
74. Lv W, Li Z J, Deng Y Q, Yang Q H, Kang F Y. Graphene-based materials for electrochemical energy storage devices: Opportunities and challenges. Energy Storage Materials, 2016, 2: 107–138
75. Yang X, Cheng C, Wang Y, Qiu L, Li D. Liquid-mediated dense integration of graphene materials for compact capacitive energy storage. Science, 2013, 341(6145): 534–537
76. El-Kady M F, Strong V, Dubin S, Kaner R B. Laser scribing of high-performance and flexible graphene-based electrochemical capacitors. Science, 2012, 335(6074): 1326–1330
77. El-Kady M F, Kaner R B. Scalable fabrication of high-power graphene micro-supercapacitors for flexible and on-chip energy storage. Nature Communications, 2013, 4: 1475
78. Gao W, Singh N, Song L, Liu Z, Reddy A L M, Ci L, Vajtai R, Zhang Q, Wei B, Ajayan P M. Direct laser writing of micro-supercapacitors on hydrated graphite oxide films. Nature Nanotechnology, 2011, 6(8): 496–500
79. Yan Z X, Zhang Y L, Wang W, Fu X Y, Jiang H B, Liu Y Q, Verma P, Kawata S, Sun H B. Superhydrophobic SERS substrates based on silver-coated reduced graphene oxide gratings prepared by two-beam laser interference. ACS Applied Materials & Interfaces, 2015, 7(49): 27059–27065
80. Wan X, Huang Y, Chen Y. Focusing on energy and optoelectronic applications: a journey for graphene and graphene oxide at large scale. Accounts of Chemical Research, 2012, 45(4): 598–607
81. Ding X, Liu H, Fan Y. Graphene‐based materials in regenerative medicine. Advanced Healthcare Materials, 2015, 4(10): 1451–1468
82. Guo W, Wang S, Yu X, Qiu J, Li J, Tang W, Li Z, Mou X, Liu H, Wang Z. Construction of a 3D rGO-collagen hybrid scaffold for enhancement of the neural differentiation of mesenchymal stem cells. Nanoscale, 2016, 8(4): 1897–1904
83. Lorenzoni M, Brandi F, Dante S, Giugni A, Torre B. Simple and effective graphene laser processing for neuron patterning application. Scientific Reports, 2013, 3(1): 1954
84. Peláez R J, González-Mayorga A, Gutiérrez M C, García-Rama C, Afonso C N, Serrano M C. Tailored fringed platforms produced by laser interference for aligned neural cell growth. Macromolecular Bioscience, 2016, 16(2): 255–265
85. Tao W, Zhu X, Yu X, Zeng X, Xiao Q, Zhang X, Ji X, Wang X, Shi J, Zhang H, Mei L. Black phosphorus nanosheets as a robust delivery platform for cancer theranostics. Advanced Materials, 2017, 29(1): 1603276
86. Sun Z, Xie H, Tang S, Yu X F, Guo Z, Shao J, Zhang H, Huang H, Wang H, Chu P K. Ultrasmall black phosphorus quantum dots: synthesis and use as photothermal agents. Angewandte Chemie International Edition, 2015, 54(39): 11526–11530
87. Shao J, Xie H, Huang H, Li Z, Sun Z, Xu Y, Xiao Q, Yu X F, Zhao Y, Zhang H, Wang H, Chu P K. Biodegradable black phosphorus-based nanospheres for *in vivo* photothermal cancer therapy. Nature Communications, 2016, 7: 12967
88. Gan Z, Cao Y, Evans R A, Gu M. Three-dimensional deep sub-diffraction optical beam lithography with 9 nm feature size. Nature Communications, 2013, 4: 2061
89. Lin H, Jia B, Gu M. Dynamic generation of Debye diffraction-limited multifocal arrays for direct laser printing nanofabrication. Optics Letters, 2011, 36(3): 406–408

Tieshan Yang received his Bachelor degree in Applied Physics from Ludong University, China in 2012 and his Master degree in Optical Engineering from Beijing University of Technology, China in 2015. He is now a PhD student under the supervision of Prof. Baohua Jia at Swinburne University of Technology, Australia. His research interests focus on laser nanofabrication on 2D materials for functional photonics devices.

Han Lin received his B.Sc. (2005) and M. Sc. (2008) degrees from Xiamen University, China. He was awarded a PhD (2013) from Swinburne University of Technology, Australia. He has dedicated interest and experience on optical system design and dynamic control of light-matter interaction, vectorial diffraction theory and super-resolution. He is currently working as the Postdoctoral Research Fellow at Swinburne University of Technology. His research interests focus on light-matter interaction on 2D materials and the applications in the energy storage devices and molecular separation.

Baohua Jia is a full Professor and Research Leader at Swinburne University of Technology. She received her B.Sc. (2000) and M. Sc. (2003) degrees from Nankai University, China. She was awarded a PhD (2007) from Swinburne University of Technology, Australia. She is the Head of Laser and Nanomaterial Interaction (LNI) Group. She uses light to develop various functional nanostructures to effectively harness and store clean energy and boost the performance of communication and imaging devices.